Article

Cell Stem Cell

Yin Yang 1 Orchestrates a Metabolic Program Required for Both Neural Crest Development and Melanoma Formation

Graphical Abstract

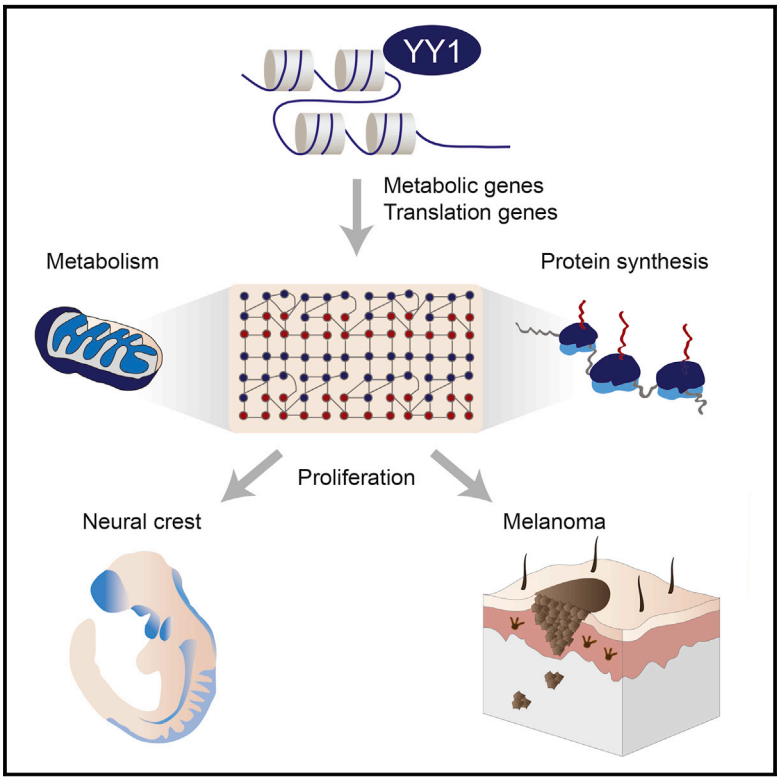

Highlights

- Yy1 regulates a transcriptional program required for early neural crest development
- Depletion of one *Yy1* allele is sufficient to prevent melanoma initiation
- YY1 regulates metabolism and translation in neural crest and melanoma
- YY1 acts upstream of MITF and c-MYC in a subset of human melanomas

Authors

Sandra Varum, Arianna Baggiolini, Luis Zurkirchen, ..., Nicola Zamboni, Reinhard Dummer, Lukas Sommer

Correspondence

lukas.sommer@anatomy.uzh.ch

In Brief

Varum and colleagues show that the transcription factor YY1 is required for both Neural Crest (NC) development and melanoma formation by regulating metabolism and translation. However, melanoma cells display increased dependency on YY1 compared to NC cells from which melanoma develops.

Varum et al., 2019, Cell Stem Cell *24*, 637–653
April 4, 2019
https://doi.org/10.1016/j.stem.2019.03.011

CellPress

Cell Stem Cell
Article

Yin Yang 1 Orchestrates a Metabolic Program Required for Both Neural Crest Development and Melanoma Formation

Sandra Varum,[1] Arianna Baggiolini,[1,7] Luis Zurkirchen,[1,7] Zeynep Kalender Atak,[2,3] Claudio Cantù,[4] Elisa Marzorati,[1] Raphaël Bossart,[1] Jasper Wouters,[2,3] Jessica Häusel,[1] Eylül Tuncer,[1] Daniel Zingg,[1] Dominiek Veen,[1] Nessy John,[1] Marcel Balz,[1] Mitchell P. Levesque,[5] Konrad Basler,[4] Stein Aerts,[2,3] Nicola Zamboni,[6] Reinhard Dummer,[5] and Lukas Sommer[1,8,*]

[1]Institute of Anatomy, University of Zurich, 8057 Zurich, Switzerland
[2]VIB Center for Brain & Disease Research, Laboratory of Computational Biology, 3000 Leuven, Belgium
[3]Department of Human Genetics, KU Leuven, 3000 Leuven, Belgium
[4]Institute of Molecular Life Sciences, University of Zurich, 8057 Zurich, Switzerland
[5]Department of Dermatology, University of Zurich Hospital, 8091 Zurich, Switzerland
[6]Institute of Molecular Systems Biology, ETH Zurich, 8093 Zurich, Switzerland
[7]These authors contributed equally
[8]Lead Contact
*Correspondence: lukas.sommer@anatomy.uzh.ch
https://doi.org/10.1016/j.stem.2019.03.011

SUMMARY

Increasing evidence suggests that cancer cells hijack developmental programs for disease initiation and progression. Melanoma arises from melanocytes that originate during development from neural crest stem cells (NCSCs). Here, we identified the transcription factor Yin Yang 1 (Yy1) as an NCSCs regulator. Conditional deletion of *Yy1* in NCSCs resulted in stage-dependent hypoplasia of all major neural crest derivatives due to decreased proliferation and increased cell death. Moreover, conditional ablation of one *Yy1* allele in a melanoma mouse model prevented tumorigenesis, indicating a particular susceptibility of melanoma cells to reduced Yy1 levels. Combined RNA sequencing (RNA-seq), chromatin immunoprecipitation (ChIP)-seq, and untargeted metabolomics demonstrated that YY1 governs multiple metabolic pathways and protein synthesis in both NCSCs and melanoma. In addition to directly regulating a metabolic gene set, YY1 can act upstream of MITF/c-MYC as part of a gene regulatory network controlling metabolism. Thus, both NCSC development and melanoma formation depend on an intricate YY1-controlled metabolic program.

INTRODUCTION

The neural crest (NC) is a distinctive embryonic stem cell population central to the evolution of vertebrates and is endowed with one of the broadest differentiation potentials *in vivo* (Baggiolini et al., 2015; Dupin and Sommer, 2012). NC cells can give rise to a plethora of cell types, ranging from the craniofacial mesenchyme to neurons and glia of the peripheral nervous system and skin melanocytes. Melanoma arises from the neoplastic transformation of melanocytes and is frequently driven by BRAF and NRAS mutations (Akbani et al., 2015).

Recent reports suggest that, for disease initiation, progression, and drug resistance, cancer cells reuse aspects of native developmental programs. Several transcription factors (TFs) that allow cellular reprogramming and unlimited self-renewal are bona fide oncogenes (Suvà et al., 2013). For instance, skin squamous-cell carcinoma initiation is marked by the reactivation of an embryonic epidermis transcriptional program orchestrated by the stem cell TF Sox2 (Boumahdi et al., 2014). Moreover, a core of neurodevelopmental TFs is essential for glioblastoma propagation (Suvà et al., 2014). However, in melanoma, Sox2 is required for neither tumor initiation nor disease progression (Schaefer et al., 2017). Moreover, melanoma cells reprogrammed into cells with features of induced pluripotent stem cells gave rise to teratomas *in vivo* rather than to melanomas, suggesting that a lineage-specific stem cell program may determine cancer identity (Bernhardt et al., 2017). When fully differentiated, reprogrammed melanoma cells lost their tumorigenic potential despite their oncogenic load, indicating that a progenitor program might be required for tumorigenesis (Bernhardt et al., 2017). In agreement with this idea, the NC lineage TF SOX10 is recurrently overexpressed in human melanoma and down-modulation of this TF is sufficient to prevent melanoma initiation in a murine model (Shakhova et al., 2012). Melanoma initiation in a *BRAF^{V600E};P53*-deficient zebrafish melanoma model is accompanied by the re-expression of NC progenitor markers (Kaufman et al., 2016). Moreover, acquired resistance to RAF and MEK inhibition in melanoma patients has been linked to the emergence of a cell population expressing NC markers (Rambow et al., 2018). Thus, it is conceivable that the tumorigenic and migratory potential of melanoma cells depends on the attainment of a developmental program required for NC.

In this study, we identified the TF Yin Yang 1 (YY1) as a master regulator of a NC transcriptional program. Intriguingly, Yy1 is not only required for NC survival and proliferation at early embryonic

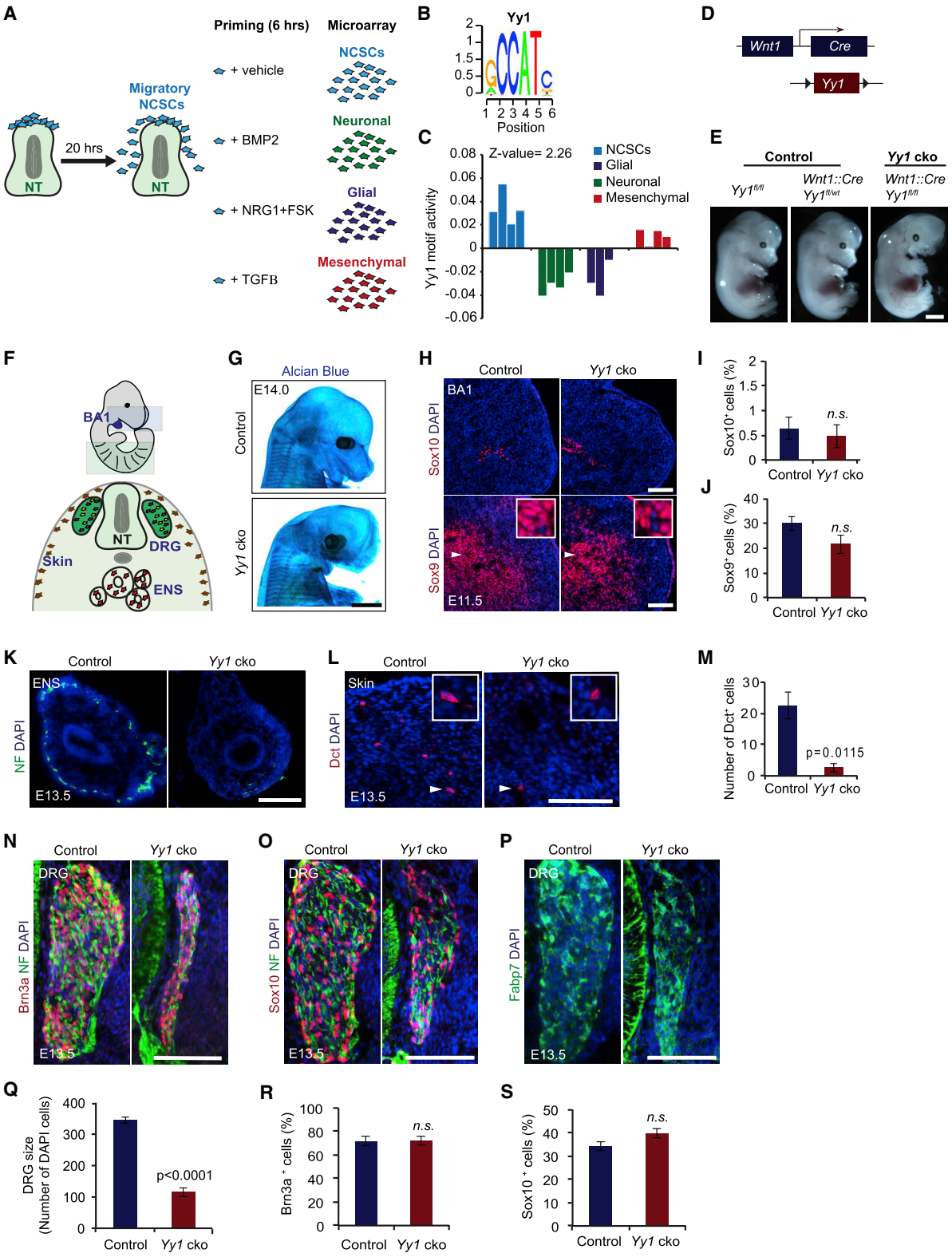

Figure 1. Yy1 Is Required for Early NC Development

(A) Strategy used to identify TFs involved in NCSC maintenance.

(B and C) ISMARA analysis (Balwierz et al., 2014) identified the Yy1 motif (B) being enriched in NCSCs compared to differentiated counterparts (C). Bar graph represents Yy1 motif activity in the different biological replicates.

(legend continued on next page)

stages but also for tumor initiation in a genetically engineered melanoma mouse model. Mechanistically, YY1 binds and regulates a large subset of genes involved in general metabolic processes, thus controlling various metabolic pathways as well as protein synthesis rates both during NC development and in melanoma.

RESULTS

NCSCs Display High Yy1 Motif Activity

NC stem cells (NCSCs) can be primed to differentiate into specific cell fates by the use of instructive growth factors (Dupin and Sommer, 2012). To identify players in NCSC maintenance, we performed a differential gene expression analysis in migratory NCSCs and NC cells primed to differentiate into mesenchymal, neuronal, and glial lineages (Figure 1A). We next asked which TF could act as a master regulator of this transcriptional program by applying an integrated motif activity response analysis (ISMARA) to the resulting dataset (Balwierz et al., 2014). This analysis showed that NCSCs display higher Yy1, E2f, and Nfy motif activities than their primed counterparts, suggesting a possible role for these TFs in NCSC maintenance (Figures 1B and 1C; data not shown). Because Yy1 motif activity best discriminated NCSCs from their differentiated counterparts, we decided to focus our analysis on Yy1, a broadly expressed TF that can regulate gene expression by facilitating promoter-enhancer interactions (Weintraub et al., 2017).

Yy1 Is Essential for Early NC Development *In Vivo*

To address the *in vivo* requirements of Yy1 during NC development, we crossed mice homozygous for the floxed allele of *Yy1* (Affar et al., 2006) with mice carrying a transgene expressing Cre recombinase under the *Wnt1* promoter (Danielian et al., 1998; Figure 1D). This strategy allowed us to specifically and efficiently deplete *Yy1* in pre-migratory NC cells (Figures S1A and S1B). Although *Yy1* conditional knockout (cko) embryos perished around embryonic day 14.5 (E14.5), *Wnt1::Cre*;$Yy1^{fl/wt}$ embryos were viable and developed into fertile offspring indistinguishable from their wild-type littermates (Figures 1E and S1C; data not shown).

Gross morphological analysis of *Yy1* cko embryos revealed marked midbrain and craniofacial defects consistent with the pattern of *Wnt1::Cre* expression (Danielian et al., 1998) and a requirement of Yy1 for the morphogenesis of NC-derived mesenchyme (Figure 1E). Alcian Blue staining of *Yy1* cko embryos showed loss of virtually all NC-derived chondrogenic craniofacial structures (Figures 1F and 1G). The acquisition of mesenchymal fates by NCSCs has been associated with loss of Sox10 and the acquisition of the mesenchymal marker Sox9 (John et al., 2011). In branchial arch (BA) 1 of *Yy1* cko embryos at E11.5, expression of these TFs was unaltered, suggesting that the craniofacial defects observed upon *Yy1* cko are not due to an overt differentiation defect (Figures 1H–1J).

In agreement with a requirement for Yy1 in NCSC maintenance, the depletion of *Yy1* also affected the development of other NC derivatives (Figures 1F and 1K–1Q). Absence of the pan-neuronal marker neurofilament (NF) in E11.5 and E13.5 gut cross-sections revealed that *Yy1* cko NCSCs fail to form the enteric nervous system (Figures 1K and S1D). Moreover, analysis of the melanocytic marker Dct showed a marked reduction in melanocyte numbers in *Yy1* cko embryos (Figures 1L and 1M). Finally, E13.5 *Yy1* cko embryos displayed a significant reduction in the size of dorsal root ganglia (DRG) (Figures 1N–1Q). However, immunohistochemistry for the sensory neuronal marker Brn3a, NF, and the satellite glial marker FABP7 demonstrated normal differentiation of *Yy1* cko DRG cells (Figures 1N, 1P, 1R, S1E, and S1F). Similarly, the relative numbers of *Yy1*-deficient post-migratory NCSCs and glial cells marked by Sox10 were only modestly reduced at E11.5 and back to normal levels at E13.5 (Figures S1G, S1H, and 1S). Collectively, these results demonstrate that depletion of *Yy1* in pre-migratory NCSCs results in agenesis or reduction of multiple NC derivatives, although NCSC differentiation is not impaired.

Yy1 Controls Proliferation and Survival of NC Cells in a Stage-Dependent Manner *In Vivo*

The phenotype observed upon depletion of *Yy1* in pre-migratory NCSCs could possibly result from defective proliferation and/or decreased cell survival. Indeed, proliferation in the BA and DRG of E11.5 *Yy1* cko was impaired and cell death increased (Figures 2A–2E and 2G, 2H, and 2J). Interestingly, analysis of proliferation and apoptotic rates at E13.5 revealed rescued proliferation and reduced apoptosis (Figures 2F, 2G, 2I, and 2J).

NC derivatives harbor post-migratory NC cell populations exhibiting stem cell properties (Dupin and Sommer, 2012). To address whether Yy1 was also required for post-migratory Sox10-expressing NC cells, we crossed mice carrying floxed alleles of *Yy1* with *Sox10::CreER*^{T2} mice harboring a tamoxifen (TM)-inducible Cre recombinase under the *Sox10* promoter (Simon et al., 2012). Depletion of *Yy1* at E10.5 resulted in a marked reduction in the number of melanocytes, consistent with previous findings (Li et al., 2012; Figures S2A–S2C).

(D) Strategy used to conditionally ablate *Yy1* in pre-migratory NCSCs.
(E) Representative pictures of E13.5 control and *Yy1* cko embryos.
(F) Drawing representing the different NC derivatives analyzed.
(G) Alcian Blue staining of control and *Yy1* cko embryos.
(H–J) Immunostaining (H) and quantification of $Sox10^+$ (I) and $Sox9^+$ (J) cells in E11.5 control and *Yy1* cko BAs.
(K) Immunohistochemistry for the neuronal marker NF in E13.5 control and *Yy1* cko gut sections.
(L and M) Immunostaining (L) and quantification (M) of Dct^+ melanocytes in E13.5 control and *Yy1* cko embryos.
(N and R) Immunostaining for Brn3a and NF (N) and quantification of $Brn3a^+$ (R) in E13.5 control and *Yy1* cko DRGs.
(O, P, and S) Immunostaining for Sox10 and NF (O), Fabp7 and NF (P), and corresponding quantification of $Sox10^+$ cells (S) in the DRG.
(Q) Quantification of $DAPI^+$ cells per DRG cross-section based on (N)–(P).
Data are shown as mean ± SEM; n = 3 control and *Yy1* cko embryos derived from at least two independent litters. p values were determined with unpaired Student's t test. Scale bars: 1 mm in (E); 2 mm in (G); 100 μm in (H)–(P). Abbreviations: BA, branchial arch; DRG, dorsal root ganglia; ENS, enteric nervous system; FSK, forskolin; NRG1, neuregulin type 1; *n.s.*, not significant. See also Figure S1.

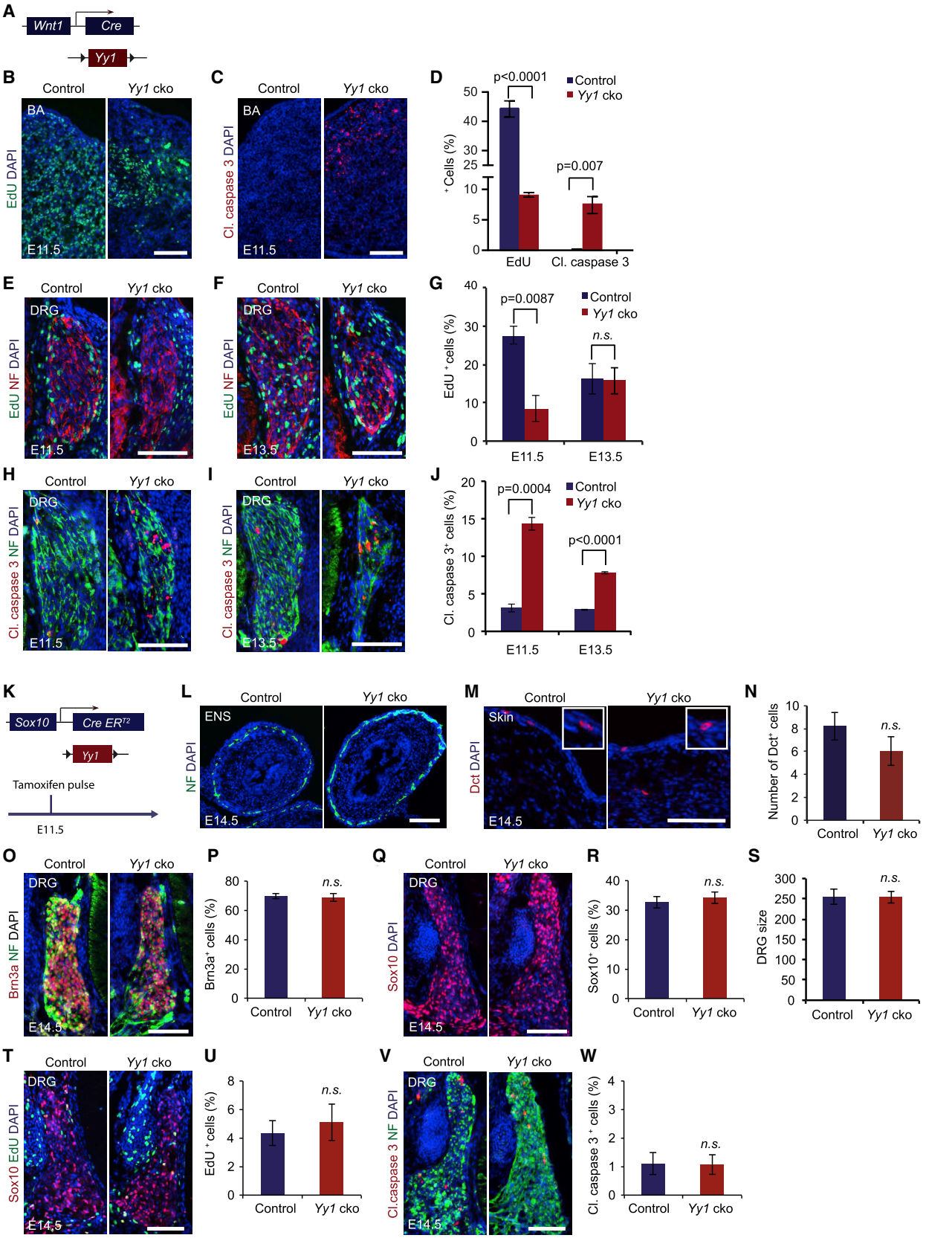

(legend on next page)

Likewise, *Yy1* cko embryos displayed reduced DRG size (Figure S2D). However, no differences in the percentage of Sox10$^+$ cells and Brn3a$^+$ cells were observed (Figures S2E–S2H). Although depletion of *Yy1* at E10.5 did not impair proliferation, it led to a transient decrease in cell survival that was resolved by E12.5 (Figures S2I–S2L). The abiding apoptosis upon *Wnt1::Cre*-mediated *Yy1* ablation when compared to *Sox10::CreER^{T2}* (Figures 2I, 2J, S2K, and S2L) could be due to targeting of differentiated neurons with the *Wnt1::Cre* line and/or to a decreased requirement of Yy1 during embryonic development.

Surprisingly, when Cre recombination was induced at E11.5, we did not observe any overt phenotype in the resulting *Yy1* cko embryos (Figures 2K–2W). There were no significant differences in the number of Dct$^+$ cells between control and *Yy1* cko embryos at E14.5 (Figures 2M and 2N). Likewise, neither proliferation (Figures 2T and 2U) nor apoptosis was affected in *Yy1* cko DRG at E14.5 (Figures 2V and 2W). Thus, unlike *Yy1* depletion at a pre-migratory stage, *Yy1* cko in post-migratory NC cells at E11.5 resulted in no obvious phenotype, indicating a stage-dependent requirement for *Yy1* during NC development.

Yy1 Is Required for Homeostasis of the Adult Melanocytic Lineage

Depletion of *Yy1* in the melanocytic lineage during embryonic development leads to a reduction in the number of melanocytes postnatally (Li et al., 2012). To determine whether Yy1 is also required for homeostasis of adult melanocytes, we conditionally ablated either one allele of *Yy1 (Yy1$^{+/-}$)* or both alleles of *Yy1 (Yy1$^{-/-}$)* specifically in the adult melanocytic lineage by using a TM-inducible *Tyr::CreER^{T2}* line (Bosenberg et al., 2006) known to drive Cre-dependent recombination in both melanocyte stem cells and in differentiated melanocytes (Harris et al., 2013; Figures 3A and 3B). Fate mapping of recombined cells was possible due to inclusion of a *ROSA26 Cre* reporter allele. Although depletion of both *Yy1* alleles resulted in hair graying, the coat color of *Yy1$^{+/-}$* animals was indistinguishable from that of control animals (Figure 3C). During anagen, *Yy1$^{-/-}$* animals had reduced numbers of melanocytes when compared to control animals, although no significant differences could be observed between control and *Yy1$^{+/-}$* animals (Figures 3D and 3E). Some tdTomato$^+$ melanocytes in *Yy1$^{-/-}$* animals still retained Yy1 protein due to incomplete Cre recombination. However, in these animals, a small subset of hair follicles contained melanocytes devoid of Yy1 expression and these presented lighter pigmentation (Figure 3G). Interestingly, analysis of tdTomato$^+$ hair bulbs per Dct$^+$ hair bulbs showed that *Yy1$^{-/-}$* animals had a reduced percentage of recombined hair follicles compared to *Yy1$^{+/-}$* animals. Our results suggest that depletion of both alleles of *Yy1* in the adult melanocytic lineage conferred a selective disadvantage to melanocyte stem cells and diminished the survival and/or proliferation rates of melanocytes (Figure 3F).

Depletion of One *Yy1* Allele Is Sufficient to Prevent Melanoma Initiation and Growth

To investigate whether Yy1 is functionally implicated in melanoma initiation, we took advantage of the cutaneous *Tyr::N-Ras^{Q61K};Cdnk2a$^{-/-}$* melanoma mouse model, which develops skin melanomas spontaneously within 6 months of age (Ackermann et al., 2005; Shakhova et al., 2012). In these mice, Yy1 was co-expressed with Dct in hair follicles, dermal hyperplasia, and skin melanomas (Figure S3A). Using *Tyr::CreER^{T2}* (Figure 4A), we conditionally depleted either one allele of *Yy1 (Yy1$^{+/-}$)* or both alleles of *Yy1 (Yy1$^{-/-}$)* at 1 month of age by injecting TM (Zingg et al., 2015; Figures 4B and S3B). Recombination efficiency was 47.07% ± 3.20%, as determined by quantifying the number of GFP-expressing cells among the total number of Dct-expressing cells in skin hyperplastic lesions. Strikingly, although control animals developed skin melanomas as expected, both *Yy1$^{+/-}$* and *Yy1$^{-/-}$* animals exhibited significantly reduced tumor burden and significantly increased melanoma tumor-specific survival (Figures 4C and 4D).

Two months after recombination, *Yy1$^{-/-}$*, but not *Yy1$^{+/-}$*, mice displayed hair pigmentation defects, reflecting deficiencies in the melanocytic lineage (Figure S3C). Therefore, we focused our further analysis on *Yy1$^{+/-}$* animals. Tracing of recombined cells by means of immunohistochemistry for GFP and DCT revealed that GFP-expressing cells could be detected in hair follicles and hyperplastic lesions, whereas virtually no recombined skin melanomas were found in *Yy1$^{+/-}$* mice (Figures 4E and 4F). Thus, depletion of one *Yy1* allele is sufficient to prevent melanoma initiation in this melanoma mouse model. To address whether Yy1 reduction was associated with reduced proliferation and increased cell death in melanoma, we isolated skin-melanoma-derived cells from control animals harboring the *Tyr::CreER^{T2};Yy1$^{fl/wt}$ Tyr::Nras^{Q61K};Cdnk2a$^{-/-}$* genotype

Figure 2. Yy1 Is Required for Proliferation and Survival of NC during Early Embryonic Development

(A) Strategy used to conditionally ablate *Yy1* in pre-migratory NCSCs.
(B and D) Staining (B) and quantification of EdU$^+$ cells (D) in E11.5 control and *Yy1* cko BAs.
(C and D) Immunostaining (C) and quantification (D) of cleaved caspase 3$^+$ cells in E11.5 control and *Yy1* cko BAs.
(E–G) EdU staining in E11.5 (E) and E13.5 (F) control and *Yy1* cko DRGs and corresponding quantifications (G).
(H–J) Immunostaining for cleaved caspase 3$^+$ in E11.5 (H) and E13.5 (I) control and *Yy1* cko DRGs and corresponding quantifications (J).
(K) Strategy used to conditionally ablate *Yy1* in E11.5 post-migratory NCSCs.
(L) Immunohistochemistry for NF in E14.5 control and *Yy1* cko gut sections.
(M and N) Immunostaining (M) and quantification (N) of Dct$^+$ melanocytes in E14.5 control and *Yy1* cko embryos (n = 4).
(O and P) Immunostaining (O) and quantification (P) of Brn3a$^+$ and NF$^+$ cells in E14.5 control and *Yy1* cko DRGs.
(Q and R) Immunostaining (Q) and quantification (R) of Sox10$^+$ cells in E14.5 control and *Yy1* cko DRGs.
(S) Quantification of DAPI$^+$ cells per DRG cross-section in E14.5 embryos.
(T and U) Staining (T) and quantification (U) of EdU$^+$ cells in E14.5 control and *Yy1* cko DRGs.
(V and W) Immunostaining (V) and quantification (W) of cleaved caspase 3$^+$ cells in E14.5 control and *Yy1* cko DRGs.
Data are shown as mean ± SEM; n = 3 control and *Yy1* cko embryos derived from at least two independent litters, unless specified otherwise. p values were determined with unpaired Student's t test. Scale bars: 100 μm. See also Figure S2.

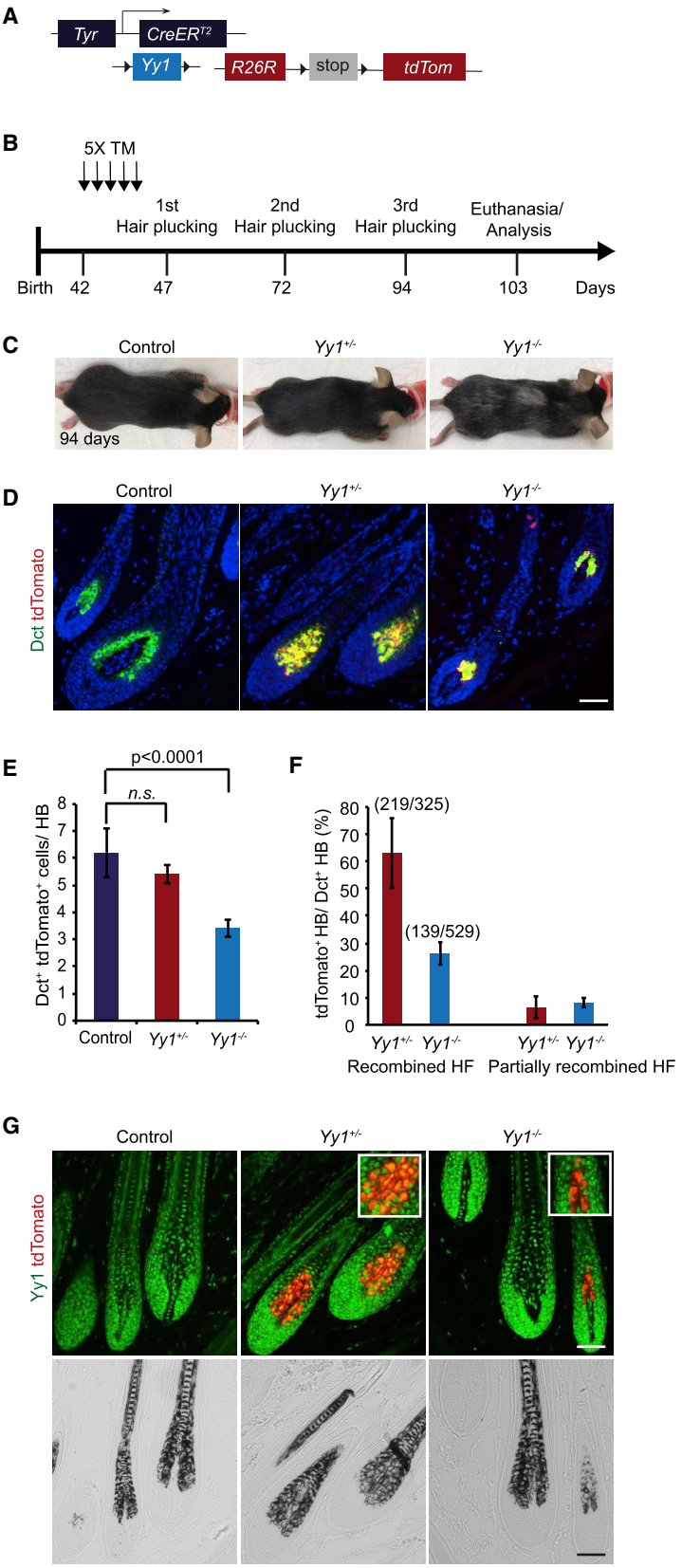

Figure 3. *Yy1* Is Required for Adult Melanocyte Homeostasis

(A and B) Mouse genotype (A) and strategy (B) used to conditionally ablate *Yy1* in the adult melanocytic lineage.

(C) Representative picture of mice coat color upon *Tyr::CreER*^{T2}-mediated depletion of either one *Yy1* allele (*Yy1*$^{+/-}$) or both *Yy1* alleles (*Yy1*$^{-/-}$).

(D and E) Immunostaining (D) and quantification (E) of Dct^{+} and tdTomato^{+} cells per hair bulb in anagen hair follicles. Data are shown as mean ± SEM; p values were determined by one-way ANOVA followed Tukey's test. At least 100 hair bulbs from 3 or more animals were quantified per genotype.

(F) Quantification of recombined hair follicles in *Yy1*$^{+/-}$ and *Yy1*$^{-/-}$ animals. Number of hair bulbs quantified is depicted in the graph.

(G) Immunohistochemistry for Yy1 and tdTomato and bright-field pictures depicting *Yy1*$^{+/-}$ and *Yy1*$^{-/-}$ representative anagen hair bulbs.

Scale bars: 100 μm. Abbreviations: HB, hair bulb; TM, tamoxifen; n.s., not significat.

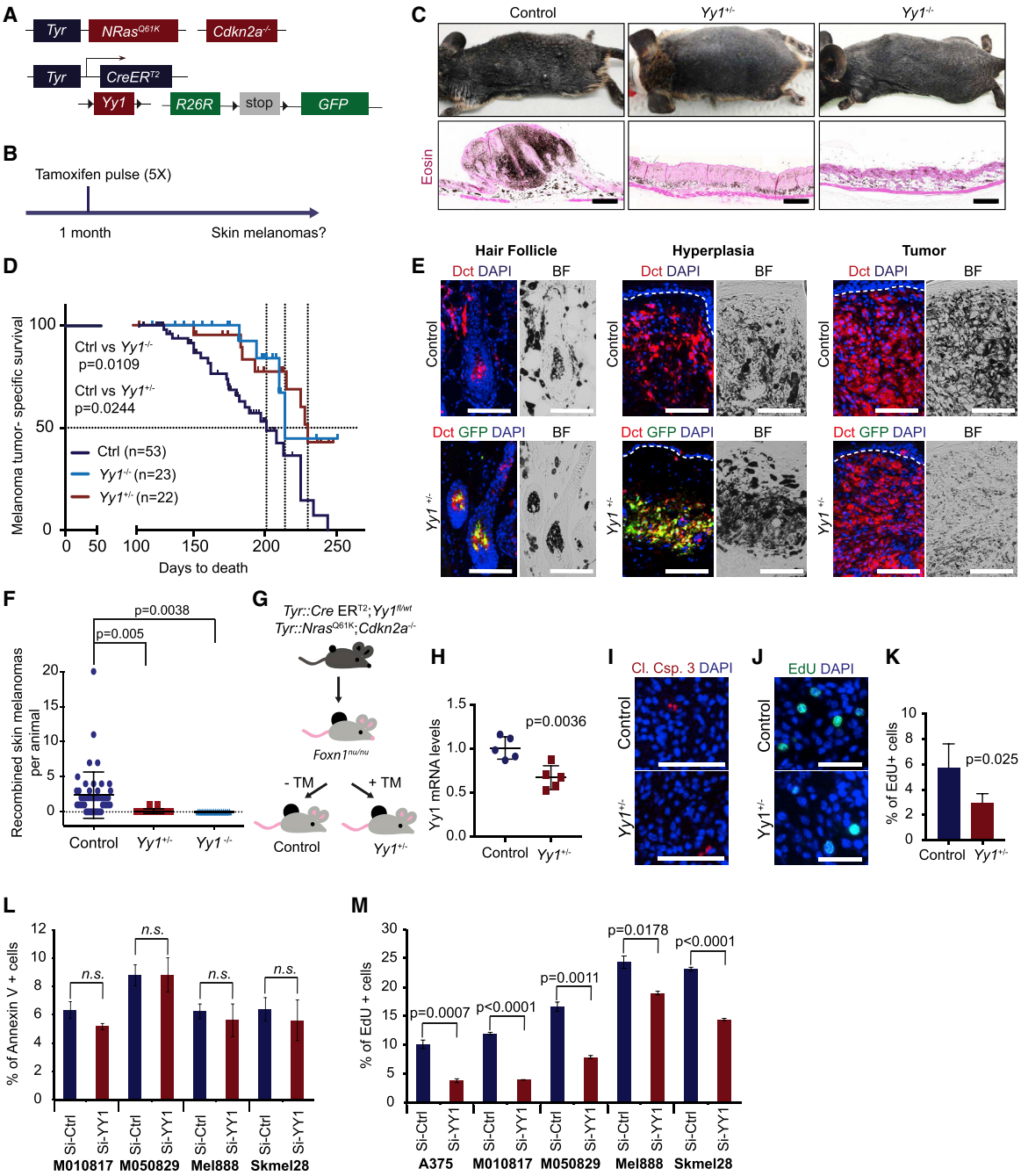

Figure 4. Depletion of One *Yy1* Allele Is Sufficient to Prevent Melanoma Initiation and Growth

(A and B) Mouse genotype (A) and strategy (B) used to conditionally ablate *Yy1* in the melanocytic lineage of the melanoma model *Tyr::Nas*^{Q61K};*Cdkn2a*$^{-/-}$.

(C) Representative animal pictures and eosin staining of skin sections.

(D) Kaplan-Meier curves comparing melanoma tumor-specific survival. p values were determined with log rank (Mantel-Cox) test.

(E) Immunohistochemistry for GFP^{+} and Dct^{+} cells in hair follicles, hyperplasia, and tumors.

(F) Quantification of recombined skin melanomas. n refers to the number of animals: control n = 50; *Yy1*$^{+/-}$ n = 18; and *Yy1*$^{-/-}$ n = 17. One-way ANOVA followed by Tukey's test.

(G) Scheme depicting the allograft of *Tyr::CreER*^{T2};*Yy1*$^{fl/wt}$; *Tyr::Nras*^{Q61K};*Cdkn2a*$^{-/-}$ cells in athymic nude-Foxn1 mice and strategy used to induce loss of one *Yy1 allele*.

(H) qRT-PCR for Yy1 in melanoma allografts. n = 5; unpaired Student's t test.

(I) Immunohistochemistry for cleaved caspase 3^{+} cells in melanoma allografts.

(J and K) Staining (J) and quantification (K) of EdU^{+} cells in melanoma allografts. Data are shown as mean ± SEM; n = 5; unpaired Student's t test.

(L and M) Flow cytometric analysis and quantification of EdU^{+} cells (M) and Annexin V^{+} (L) cells in human melanoma cells subjected to siRNA-mediated KD of YY1. Data are shown as mean ± SEM; n equals to at least 3 biological replicates; unpaired Student's t test.

Scale bars 500 μm (in C); scale bars 100 μm (in E, I, and J). See also Figure S3.

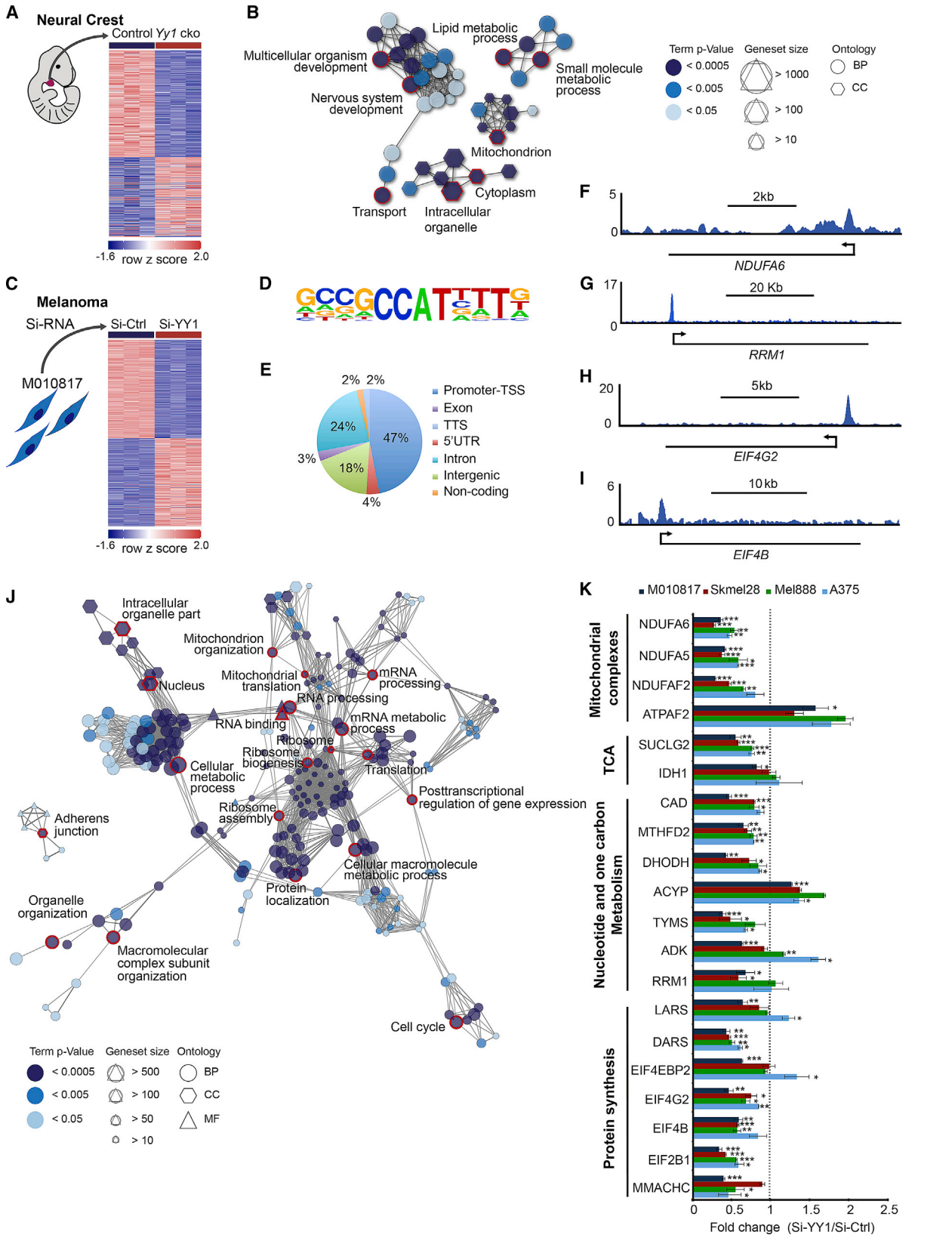

(legend on next page)

and engrafted these cells into athymic nude Foxn1^{nu} mice (Zingg et al., 2015; Figure 4G). Tumors were allowed to grow, and loss of one *Yy1* allele was induced by TM injection (Figure 4H). No differences in *Nras*^{Q61K} transgene expression were observed between control and *Yy1*$^{+/-}$ tumors (Figures S3D and S3E). Although depletion of one allele of *Yy1* did not increase cell death in already established tumors, *Yy1*$^{+/-}$ tumors exhibited decreased numbers of cells in S phase when compared to control melanomas (Figures 4I–4K).

To address the relevance of our findings in human melanoma, we reduced YY1 levels in a panel of human melanoma cell lines by small interfering RNA (siRNA)-mediated knockdown (KD) (Figures S3F and S3G). Although YY1 KD did not alter cell survival in human melanoma (Figure 4L), YY1 KD led to reduced numbers of cells in S phase (Figure 4M). Thus, as in NC cells, YY1 regulates proliferation in melanoma cells.

YY1 Binds and Regulates a Subset of Genes Involved in Metabolism and Protein Synthesis

To gain insight into the molecular mechanisms underlying the dependence of NC cells on Yy1, we performed RNA sequencing (RNA-seq) analysis in E10.5 BA1 cells of control and *Yy1* cko embryos. Clustering of biological replicates demonstrated comparable global gene expression patterns across samples of the same genotype (Figure 5A). Gene Ontology (GO) network-based cluster analysis showed that gene sets transcriptionally regulated by Yy1 are enriched in developmental and metabolic processes (Figures 5B and S4A; Table S1).

To verify that the changes in metabolic gene expression observed upon *Yy1* depletion were not due to the presence of a small population of dying cells, we analyzed the expression of a subset of metabolic genes at E9.5, when apoptosis was not yet evident (Figures S4B and S4C). Similar to E10.5 *Yy1* cko embryos, E9.5 *Yy1* cko embryos already displayed altered gene expression in metabolism-related genes (Figure S4D). Moreover, chromatin immunoprecipitation (ChIP)-qPCR for Yy1 in control E10.5 BA1 cells identified binding of Yy1 to the promoter region of metabolic and protein translation genes, consistent with previous findings (Kleiman et al., 2016; Lu et al., 2013; Perekatt et al., 2014; Figure S4E).

To address whether a similar transcriptional program was controlled by YY1 in human melanoma, we performed differential gene expression analysis by RNA-seq in a human melanoma cell line subjected to siRNA-mediated YY1 KD (Figures 5C, S3F, and S3G). In addition, we performed ChIP sequencing (ChIP-seq) analysis for YY1 to identify its direct targets in human melanoma. Peak calling in two experimental replicates identified 2,063 and 1,719 peaks (false discovery rate [FDR] $\leq$ 0.01), which were at least 2-fold enriched over input. Consistent with bona fide YY1 binding sites, the most enriched motif in these regions was the YY1 motif with a high significance score (p value < 1e−50; Figure 5D). Analysis of YY1 binding site location with HOMER demonstrated that approximately 50% of the peaks were located in the promoter region (Figure 5E). For instance, we detected YY1 binding events at the mitochondrial complex I gene *NDUFA6*, the nucleotide metabolism gene *RRM1*, and at the promoter regions of protein-synthesis-related genes (Figures 5F–5I).

To identify functional classes of YY1 direct targets, we intersected our RNA-seq and ChIP-seq datasets and performed network-based cluster analysis. This analysis unveiled cellular metabolic processes, mRNA metabolic processes, and translation-related processes to be among the most enriched functional ontologies (Figures 5J and S5; Table S1). To verify this transcriptional response to YY1 KD, we validated the expression of several genes involved in different fundamental metabolic processes by qRT-PCR in three additional human melanoma cell lines (Figure 5K). In all cell lines, YY1 KD affected a broad subset of genes associated with mitochondrial electron transfer chain (ETC), tricarboxylic acid cycle (TCA), one carbon metabolism, nucleotide metabolism, and protein synthesis (Figure 5K). Collectively, these results suggest that YY1 binds and regulates a subset of genes associated with fundamental metabolic processes both during NC development and in melanoma.

YY1 Regulates Metabolism and Protein Synthesis Rates in NC and Melanoma

We next asked whether the changes in metabolism-related gene expression observed upon YY1 depletion or KD impaired cellular metabolic processes. To analyze mitochondrial bioenergetics, we measured oxygen consumption rates (OCRs) in NC cells derived from E10.5 control and *Yy1* cko BA cells and found that loss of Yy1 leads to reduced basal OCRs and maximal respiratory capacity (Figures 6A and 6B). Further, the percentage of oxygen allocated to ATP production (ATP turnover) was decreased in *Yy1* cko cells. Importantly, similar data were obtained with human melanoma cells subjected to YY1 KD (Figures 6C, 6D, S5B, and S5C), in agreement with previous findings

Figure 5. YY1 Binds and Regulates Metabolism and Protein-Synthesis-Related Genes

(A) Heatmap depicting differential gene expression between E10.5 control and *Yy1* cko BA cells (fold change of at least 1.5 with FDR < 0.05), as determined by RNA sequencing. n = 3 control and *Yy1* cko embryos from at least two independent litters.

(B) GO network analysis of differentially regulated genes between E10.5 control and *Yy1* cko cells.

(C) Heatmap depicting differential gene expression between Si-control and Si-YY1 melanoma cells (fold change of at least 1.5 with FDR < 0.01), as determined by RNA sequencing. n = 3 biological replicates.

(D) Homer motif discovery shows the YY1 motif as the most enriched motif in YY1 binding regions (p value < 1e−50).

(E) Distribution of YY1 binding regions.

(F–I) YY1 binding events in the promoter regions of metabolic (F and G) and protein translation-related genes (H and I).

(J) GO network analysis of YY1 direct targets, which expression is altered upon YY1 KD in human melanoma (overlap between ChIP-seq and RNA-seq datasets).

(K) qRT-PCR for metabolism and protein-synthesis-related genes in different human melanoma cell lines subjected to YY1 KD. Data are shown as mean ± SEM; n equals to at least 3 biological replicates; unpaired Student's t test.

For GO network analysis: each node represents an enriched GO term (adjusted p value, corrected with Bonferroni step-down procedure p < 0.05). Nodes are interconnected when gene overlap is >50%, based on the kappa score. Abbreviations: BP, biological processes; CC, cellular compartment; MF, molecular function. *p < 0.05; **p < 0.01; ***p < 0.0001. See also Figures S4 and S5.

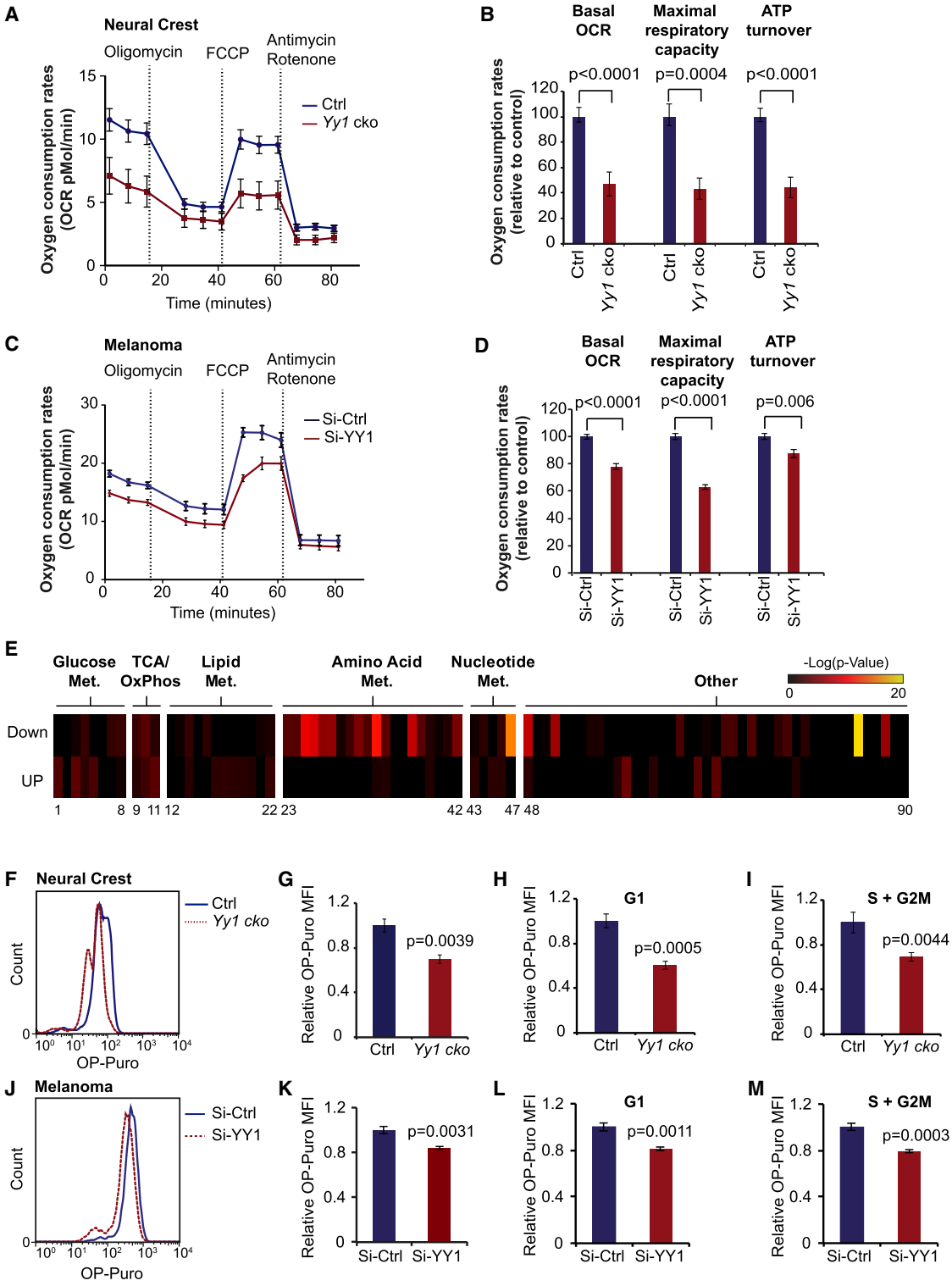

Figure 6. YY1 Regulates Metabolism and Protein Synthesis Rates in NC and Melanoma

(A and B) OCR measurements (A) and mitochongrial bioenergetics (B) in E10.5 control and *Yy1* cko BA cells. Data are shown as mean ± SEM; n refers to the number of embryos: control n = 16; *Yy*1 cko n = 9. p values were calculated by unpaired Student's t test.

(C and D) OCR measurements (C) and mitochondrial bioenergetics (D) in Si-Control and Si-YY1 human melanoma cells. Data are shown as mean ± SEM; n refers to biological replicates: Si-Ctrl n = 9; Si-YY1 n = 11. p values were calculated by unpaired Student's t test.

(legend continued on next page)

(Blättler et al., 2012). Possibly, the exacerbated OCR phenotype observed in NC cells compared to melanoma cells could be partially due to a small percentage of *Yy1* cko neural crest cells undergoing cell death during the experimental procedure (Figures 6A–6D, S5B, and S5C).

To understand whether the metabolic changes induced by YY1 KD extended beyond mitochondrial energetics, we performed mass-spectrometry-based untargeted metabolomics (Fuhrer et al., 2011). We detected a total of 1,358 ions with a distinct mass-to-charge ratio, which were putatively mapped to human metabolites based on accurate mass measurements (Table S2). Pathway enrichment analysis revealed that several metabolic pathways were disturbed upon YY1 KD, including glucose metabolism, TCA cycle, lipid metabolism, amino acid metabolism, and nucleotide metabolism (Figures 6E and S5D; Table S3), However, the extent to which specific pathways were altered varied considerably across the two cell lines analyzed, consistent with a previous study that reported metabolic heterogeneity between cancer cell lines (Dubuis et al., 2017).

In addition to metabolic genes, YY1 binds and regulates a subset of genes involved in protein translation (Figures 5H–5K). Accordingly, flow cytometric analysis of OP-Puro incorporation showed that BA cells from *Yy1* cko embryos as well as YY1 KD human melanoma cells have reduced protein synthesis rates compared to control (Figures 6F, 6G, 6J, 6K, S5E, S5F, and S5G). To ensure that the decline in protein synthesis rates was not due to defective proliferation, we analyzed OP-Puro incorporation individually in the replicating cell cycle phases (S+G2/M) and in G1 phase. Irrespective of the cell cycle phase, both *Yy1* cko NC cells and YY1 KD melanoma cells exhibited decreased protein synthesis rates (Figures 6H, 6I, 6L, 6M, S5H, and S5I). Together, these results demonstrate a role for Yy1 in regulating metabolism and protein synthesis in both NC and melanoma.

The Transition from a Normal Melanocyte to a Melanoma-Competent Melanocyte Is Associated with Metabolic Reprogramming

Although depletion of one *Yy1* allele did elicit an overt phenotype neither during NC development nor in the adult melanocytic lineage, it prevented melanoma formation. To gain insight into the mechanisms potentially underlying the increased dependence of melanoma cells on *Yy1*, we isolated tdTomato^{+}/cKit^{+} melanocytes by fluorescence-activated cell sorting (FACS) from wild-type and from *Nras*^{Q61K};*CdKn2a*$^{-/-}$ melanoma-competent animals and performed RNA-seq (Figure S6A). Network-based cluster analysis of significantly upregulated transcripts in *Nras*^{Q61K};*Cdkn2a*$^{-/-}$ melanocytes when compared to normal melanocytes unveiled that lipid metabolic processes and RNA metabolic processes were among the most enriched functional ontologies (Figure S6B). Interestingly, a subset of selected transcripts that were upregulated in *Nras*^{Q61K};*Cdkn2a*$^{-/-}$ melanocytes was downmodulated in human melanoma cells upon YY1 KD (Figure S6C). Thus, the transition from a normal melanocyte to a melanoma-competent cell appears to involve metabolic reprogramming, which can be partially reverted by YY1 inactivation.

Melanoma Cells Are Highly Susceptible to YY1 Downregulation

We next asked whether the requirement for YY1 was similar across different cancer types. To this end, we performed YY1 KD in melanoma cells (M010817 and Mel 888) and in a panel of epithelial cancer cell lines: prostate cancer (PC3 and Du 145); breast cancer (MDA-MB-231 and T-47D); colon cancer (WIDr); and adrenal carcinoma (NCI-H295R). Analysis of YY1 protein levels at different time points showed that, by 48 h, YY1 expression was reduced in all cell lines analyzed and, by 72 h, YY1 was practically absent in most cell lines (Figures S7A–S7E). However, marked YY1 downregulation (72 h) elicited a proliferative defect only in a fraction of the different cancer lines analyzed (Figure S7F). Of note, at 48 h, the only cell lines exhibiting decreased EdU incorporation upon YY1 KD were the melanoma cell lines and the PC3 line (Figure S7F). Moreover, gene expression analysis of a small subset of metabolic genes showed that responses in gene expression are heterogeneous across the different cell lines (Figure S7G). Thus, melanoma cells (possibly together with a subset of prostate cancer cells) appear to be particularly sensitive to YY1 KD with respect to proliferation.

YY1 Directly Controls Metabolism and Protein Translation by Cooperating with E2F/ETS Family Members, SOX10, and MITF

Metabolic rewiring during melanoma progression is a well-established process, which has mostly been associated with changes in glucose and glutamine utilization, mitochondrial and nucleotide metabolism, and oxidative stress responses (Haq et al., 2013; Leucci et al., 2016; Piskounova et al., 2015; Ratnikov et al., 2017; Vazquez et al., 2013; White et al., 2011). Therefore, we tested whether impaired proliferation in YY1 KD melanoma cells could be restored by supplementation with specific metabolites previously reported to be limiting for cell proliferation (Vander Heiden and DeBerardinis, 2017; Figures S7H–S7K). However, in all cases, we were unable to rescue melanoma cell proliferation upon YY1 KD, indicating that YY1

(E) Heatmap depicting enriched metabolic pathways that show altered metabolite content upon YY1 KD in human melanoma. Please refer to Table S3 for pathway annotations and p values. n = 5; p values were calculated by two tailed, heteroscedastic t test and were adjusted for FDR according to the Benjamini-Hochberg procedure.

(F) Representative histogram of OP-Puro mean fluorescence intensity (MFI) of E11.5 control and *Yy1* cko BA cells.

(G–I) OP-Puro MFI in E11.5 control and *Yy1* cko BA (G). OP-Puro MFI in G1 phase (H) and in the replicating cell cycle phases S+G2/M (I) is shown. Data are shown as mean ± SEM; n refers to the number of embryos: control n = 19; *Yy1* cko n = 8. p values were calculated by unpaired Student's t test.

(J) Representative histogram of OP-Puro MFI of Si-Ctrl and Si-YY1 human melanoma cells.

(K–M) OP-Puro MFI in Si-Control and Si-YY1 human melanoma cells (K). OP-Puro MFI in G1 phase (L) and in the replicating cell cycle phases S+G2/M (M) is shown. Data are shown as mean ± SEM; n refers to biological replicates: n = 5. p values were calculated by unpaired Student's t test.

Basal OCR, maximal respiratory capacity, and ATP turnover displayed in (B) and (D) were calculated based on (A) and (C), respectively, as previously described (Varum et al., 2011). Abbreviations: OCR, oxygen consumption rate; MFI, mean fluorescence intensity. See also Figures S5 and S6.

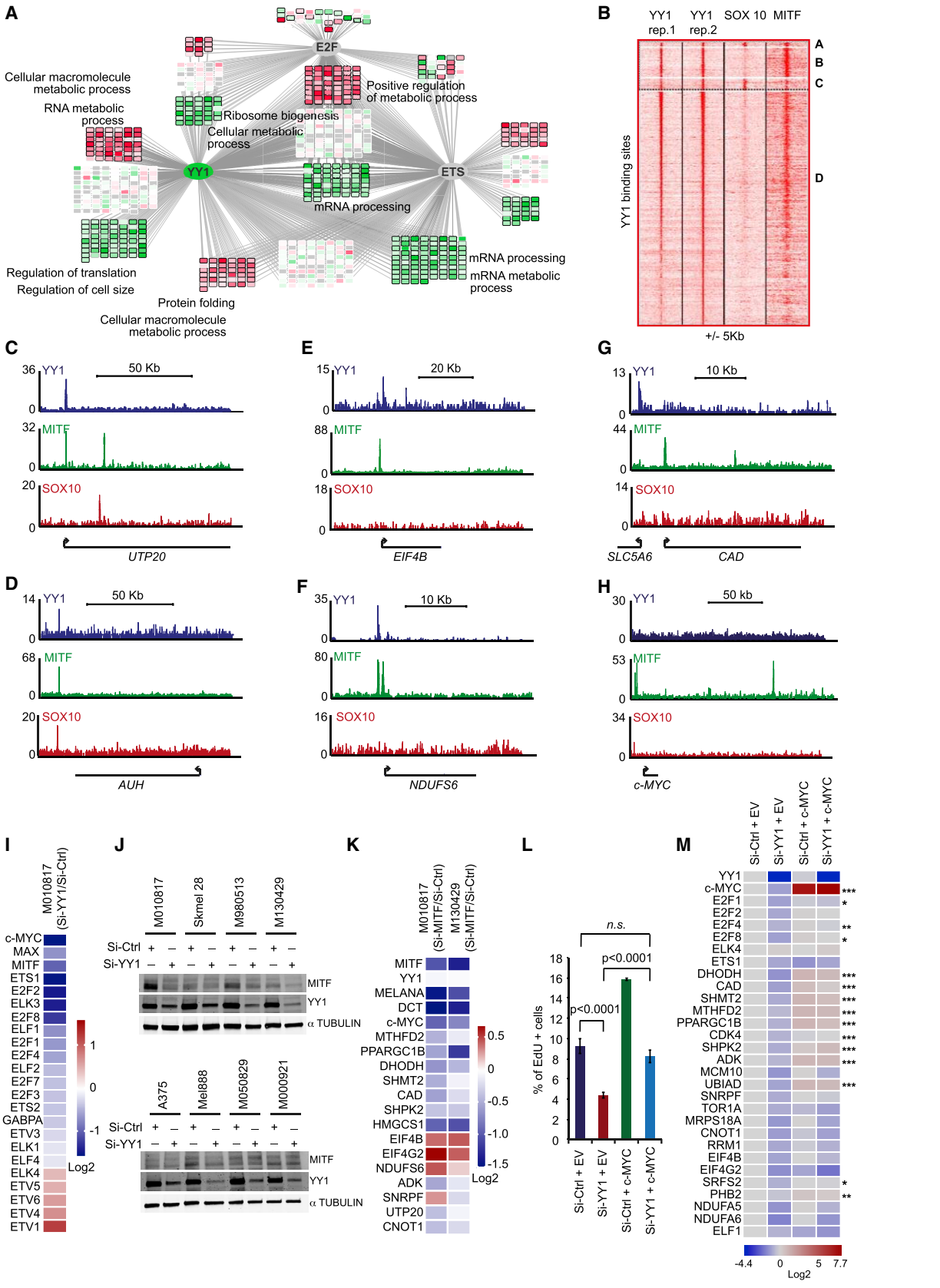

(legend on next page)

regulates multiple metabolic activities crucial for melanoma cell proliferation.

To understand how such a broad range of metabolic pathways might be controlled by YY1, we first aimed to identify putative co-factors of the YY1 gene regulatory network. To this end, we identified YY1-bound direct target genes with altered expression upon YY1 KD and reconstructed its gene regulatory network using i-cisTarget (Imrichová et al., 2015). Predicted E2F and ETS regulons (transcriptional target sets) showed the most significant overlap with the YY1 regulon (Figure 7A; Table S4). Of note, GO analysis of overlapping target genes revealed enrichment for many cellular metabolic and mRNA metabolic processes (Figure 7A).

Because E2F and ETS family members are not melanoma-specific TFs, we next asked whether part of the YY1-bound metabolic program in melanoma might involve lineage-specific co-factors. Previously, it has been shown that YY1 acquires melanocyte-lineage-specific functions by interacting with MITF (Li et al., 2012). Moreover, different combinations of MITF, SOX10, TFAP2A, and YY1 bind to a set of regulatory elements required for the melanocytic lineage (Laurette et al., 2015). Therefore, we predicted that, if YY1, MITF, and/or SOX10 were co-factors in fine-tuning metabolic gene expression in melanoma, they should co-localize in the genome. Indeed, integration of SOX10, MITF (Laurette et al., 2015; Strub et al., 2011), and YY1 ChIP-seq datasets showed that approximately 6% of YY1 bound regions were co-bound by SOX10, whereas approximately 12% of the YY1 bound regions were co-occupied by MITF (Figure 7B). Although we observed binding of YY1 neither to *MITF* nor to *SOX10* promoter or enhancer regions, we detected co-binding of YY1 in different combinations with SOX10 and MITF to protein translation or RNA-processing-related genes, such as *UTP20*, *AUH*, and *EIF4B*, and to genes encoding mitochondrial subunits, such as *NDUFS6* (Figures 7C–7F). MITF binding events were also observed for indirect targets of YY1, such as the nucleotide metabolism gene *CAD*, the folate metabolism gene *MTHFD2*, and the well-known metabolic regulator *c-MYC* (Stine et al., 2015; Figures 7G, 7H, and S7L). Moreover, GO analysis of MITF and YY1 co-bound regions revealed RNA, mitochondrial, and lysosome metabolic processes to be enriched (Figure S7M).

YY1 Acts Upstream of MITF and Regulates c-MYC and Some of Its Cognate Metabolic Targets in a Subset of Human Melanomas

Metabolic stress can suppress MITF expression as demonstrated by glutamine and glucose limitation experiments (Falletta et al., 2017; Ferguson et al., 2017). Accordingly, YY1 KD in a human melanoma cell line not only decreased the expression of various E2F, ETS, and MYC family members but also that of MITF (Figure 7I). Moreover, YY1 KD reduced MITF protein levels in some melanoma cell lines (Figure 7J). We next asked whether, in a subset of human melanomas, MITF downregulation could partially explain changes in metabolic gene expression resulting from indirect regulation by YY1. Indeed, MITF KD in human melanoma not only reduced melanocytic gene expression but also altered the expression of a subset of metabolic genes (Figure 7K). For instance, we observed changes in expression of genes co-bound by YY1 and MITF (such as *EIF4B*, *EIF4G2*, *ADK*, *CNOT1*, and *UTP20*) and of genes only bound by MITF, including c-MYC and some of its well-known targets (such as *CAD* and *MTHFD2*; Figure 7K).

MITF levels have to be tightly regulated, and MITF overexpression is known to induce cell cycle arrest (Carreira et al., 2005). Accordingly, MITF overexpression failed to rescue proliferation of YY1 KD melanoma cells (data not shown). Therefore, we sought to assess whether the MITF target c-MYC might mediate part of the YY1-induced proliferation phenotype. Apart from regulating a plethora of genes involved in fundamental metabolic processes (Stine et al., 2015), c-MYC also controls the expression of E2F family members (Zeller et al., 2006). Overexpression of c-MYC in melanoma cells was sufficient to partially rescue proliferation in YY1 KD melanoma cells (Figure 7L), which was accompanied by restored expression of some E2F family members (Figure 7M; Table S4). In addition, the expression of the metabolic genes *CAD*, *MTHFD2*, *SHMT2*, *PPARGC1B*, and *DHODH*, known to be c-MYC targets, but not directly bound by YY1, was restored (Figure 7M; Table S4). In contrast, most YY1 direct target genes belonging to the YY1/E2F/ETS/MITF transcriptional network were not rescued by c-MYC overexpression, suggesting that YY1 and/or additional TFs are required for the expression of those genes (Figure 7M). In sum, YY1 controls

Figure 7. YY1 Is Part of a Gene Regulatory Network that Controls Metabolism and Tumor Proliferation

(A) Gene regulatory network depicting YY1 and E2F and ETS family members. Node colors indicate up (red) and down (green) regulation upon YY1 KD. Nodes with black borders correspond to genes that have significant differential expression (FDR < 0.05).

(B) Read density clustering of YY1, SOX10, and MITF showing co-occupied genomic regions. A: YY1 SOX10 MITF co-occupied sites; B: YY1 MITF co-occupied sites; C: YY1 SOX10 co-occupied sites; and D: YY1 only occupied sites are shown. Peak calling for YY1, SOX10, and MITF ChIP-seq datasets was performed with MACS software using p value cutoff of 0.05.

(C–F) Diagram illustrating co-binding of YY1 in different combinations with SOX10 and/or MITF to genomic regions associated with protein translation genes (C, D, and E) and metabolic genes (F).

(G and H) Diagram illustrating MITF binding events in genomic regions not bound by YY1, namely in the promoter region of a nucleotide metabolism gene (G) and in a putative c-MYC enhancer (H).

(I) Heatmap depicting gene expression changes for a subset of selected genes in M010817 Si-YY1 versus Si-control RNA-seq (ENA: PRJEB21636).

(J) Western blot analysis of MITF protein levels upon siRNA-mediated YY1 KD in human melanoma cells.

(K) qPCR analysis of a subset of metabolic genes in melanoma cells infected with Ad-H1-Si-Ctrl or Ad-H1-Si-MITF viral particles. Heatmap depicts gene expression changes. n = 3 biological replicates.

(L) Flow cytometric analysis of EdU incorporating cells upon YY1 KD and c-MYC overexpression. Data are shown as mean ± SEM; n = 5 biological replicates. p values were calculated by one-way ANOVA followed by Tukey's test.

(M) qRT-PCR of a subset of metabolic genes in YY1 KD melanoma cells subjected to YY1 KD and c-MYC overexpression. Heatmap depicts gene expression changes. n = 3 biological replicates. Significance illustrated in the figure refers to comparison between Si-YY1 + empty vector and Si-YY1 + c-MYC. Please see Table S4 for complete statistical analysis. *p < 0.05; **p < 0.001; ***p < 0.0001.

Abbreviations: EV, empty vector; Rep1/2, replicate 1/2. See also Figure S7.

metabolic processes crucial for tumor cell proliferation both by directly binding to a subgroup of metabolic genes and, in a subset of human melanomas, by controlling a MITF and c-MYC-regulated gene set.

DISCUSSION

In this study, we identified the TF Yy1 as a master regulator of an embryonic NC transcriptional program required for maintenance and proliferation of early NC cells, although dispensable for late-stage NC cell proliferation. Remarkably, a functionally equivalent YY1-controlled program is also required for melanoma initiation and growth. However, melanoma cells are more susceptible to reduced YY1 levels than NC cells and adult melanocytes, suggesting a strict dependency of melanoma formation on mechanisms active in embryonic NC cells.

Notably, maintenance and expansion of progenitor cells, but not lineage determination and early differentiation steps, were affected in NC derivatives of *Yy1* cko embryos. This function appears to be specific for a relatively narrow time window during NC development. After NC migration, conditional ablation of *Yy1* in the melanocytic lineage resulted in skin pigmentation defects postnatally, whereas depletion of *Yy1* in the Schwann cell lineage led to hypomyelination without affecting survival or proliferation (Li et al., 2012; He et al., 2010). Likewise, we show that *Yy1* ablation in E11.5 post-migratory, Sox10-expressing NC cells did not result in an overt proliferation or survival phenotype. This is consistent with previous findings revealing differential responsiveness of early and late NCSCs to mitogenic factors (Fuchs et al., 2009). Our data do not exclude the possibility of Yy1 being required in NC derivatives at a later embryonic stage or even in adult NC-derived lineages. In fact, depletion of Yy1 in E11.5 post-migratory NC cells did not affect melanoblast formation in the embryo, although Yy1 depletion in the adult melanocyte lineage perturbed melanocyte homeostasis.

Our finding that YY1, apart from regulating embryonic NC cell proliferation, also controls melanoma cell proliferation and tumorigenesis supports the notion that melanoma-initiating cells reuse aspects of developmental programs. In a zebrafish model, melanoma initiation is invariably associated with the acquisition of crestin, a zebrafish NC progenitor marker (Kaufman et al., 2016). Moreover, inactivation of the NC TF Sox10 counteracts melanoma formation (Kaufman et al., 2016; Shakhova et al., 2012). Our study now adds another twist to this theme by emphasizing and functionally validating the importance of YY1-regulated metabolic processes for both NC development and melanoma formation. In fact, YY1 directly binds and regulates a large subset of genes implicated in metabolism and protein synthesis. Consistent with this, depletion of *Yy1* during embryonic development or reduction of YY1 protein levels in human melanoma cells resulted in impaired mitochondrial bioenergetics and altered metabolite content across multiple metabolic pathways.

The relevance of YY1 for NC development is underscored by the fact that in humans loss-of-function mutations in YY1 mainly lead to congenital craniofacial dysmorphisms, apart from neurological defects (Gabriele et al., 2017). Because melanoma is a cancer of NC origin, it is plausible that melanoma and NC cells share a high susceptibility to YY1 deregulation. Indeed, depletion of YY1 across a panel of different cancer types showed that melanoma is particularly sensitive to reduced YY1 levels. Likewise, NC and melanoma are particularly responsive to certain metabolic alterations. Several congenital diseases, mainly characterized by defects in NC derivatives, are associated with alterations in pyrimidine biosynthesis, one carbon metabolism, or ribosome biogenesis (Ng et al., 2010; Ross and Zarbalis, 2014; Wilcox et al., 2007). For instance, patients with Miller's syndrome exhibit, among others, craniofacial defects due to mutations in *DHODH*, which encodes a key enzyme involved in pyrimidine biosynthesis (Ng et al., 2010). Inhibition of DHODH impairs transcriptional elongation of a gene set required both for NC development and melanoma initiation (White et al., 2011). Although DHODH is not a direct YY1 target, YY1 KD reduced DHODH expression, possibly involving direct regulation of DHODH by MITF/c-MYC. However, despite the proven role of nucleotide metabolism in NC and melanoma, exogenous supplementation with uridine and other nucleotide analogs did not restore proliferative capacity in YY1 KD cells, indicating that additional metabolic pathways are implicated in mediating YY1 function.

In addition to metabolism-related genes, YY1 binds and regulates a subset of genes involved in protein synthesis, and depletion or reduction of Yy1 led to reduced protein synthesis rates both during NC development and melanoma. NC cells are particularly affected by ribosome biogenesis defects (Ross and Zarbalis, 2014). Moreover, cancer cells display high rates of protein synthesis, and disruption of protein translation frequently impairs tumorigenesis (Barna et al., 2008; Feng et al., 2015; Ruggero, 2013; Signer et al., 2014). Therefore, it is plausible that downregulation of protein synthesis by *Yy1* depletion not only contributes to the observed NC phenotype but also impairs melanoma initiation.

Although YY1 regulated metabolism both in NC and melanoma, susceptibility to *Yy1* genetic dosage was different: while depletion of one *YY1* allele was sufficient to prevent melanoma initiation and reduce proliferation, it neither impaired NC development nor homeostasis of normal adult melanocytes. At the gene expression level, the metabolism of a tumor resembles that of the lineage of origin (Hu et al., 2013). Furthermore, pathways that are required for biomass production are often upregulated in cancer (Ruggero, 2013; Vander Heiden and DeBerardinis, 2017). Our experiments indicate that the transition from a melanocyte to a melanoma-competent cell involves metabolic reprogramming. Intriguingly, YY1 KD in human melanoma cells partially reverted the gene expression changes observed upon transition from a melanocyte to a melanoma-competent cell. Thus, in particular in a nutrient-limiting microenvironment, melanoma cells appear to be highly dependent on metabolic and protein synthesis pathways, pointing to melanoma-specific vulnerabilities.

Reconstruction of the YY1 transcriptional network in human melanoma revealed that E2F and ETS family members are putative YY1 co-factors. These findings are in agreement with E2f motif activity being higher in NCSCs than in their differentiated counterparts and are consistent with a previous implication of E2f/Ets family members in an NC gene regulatory network (Simões-Costa et al., 2014). Because E2F and ETS family members are not lineage-specific TFs, YY1 appears to control a

metabolic program to which melanoma and NC are particularly addicted.

Historically, metabolism was considered to be a housekeeping process in the cell. However, there is increasing evidence that metabolic processes may not only be "tailored" to different cell types but might actually act as drivers for lineage specification and differentiation. Moreover, lineage-specific TFs have been shown to enhance cancer cell fitness by modulating metabolic processes. For instance, MITF enhances mitochondrial metabolism by interacting with PGC1α in a subset of human melanomas (Haq et al., 2013; Vazquez et al., 2013). The human melanoma-specific long-non-coding RNA SAMMSON is required for melanomagenesis by enhancing protein translation (Leucci et al., 2016; Vendramin et al., 2018). Indeed, we found that a subset of genes bound by YY1 is also co-bound by MITF and/or SOX10. Therefore, some of the YY1-dependent metabolic processes can be fine-tuned in conjunction with MITF, SOX10, or both during melanoma initiation and proliferation.

In a subset of human melanomas, YY1 KD resulted in downregulation of MITF protein levels. Because MITF is not a direct target of YY1, our results indicate that metabolic stress can elicit a lineage-specific response. In this context, MITF KD led to downregulation of c-MYC and several of its well-known metabolic targets. Moreover, c-MYC overexpression was sufficient to partially rescue the proliferation defects imposed by YY1 KD. This is in line with the fact that c-Myc is part of the NC specifier network and controls the size of the pre-migratory NCSC population (Kerosuo and Bronner, 2016). Of note, in melanoma, c-MYC is a convergent downstream effector of resistance and c-MYC gene signatures are restored during tumor relapse and associated with metabolic vulnerabilities (Singleton et al., 2017).

In sum, our study shows that YY1 directly regulates a wide range of metabolic processes and that NC development and melanoma are particularly sensitive to disturbance of these processes. In addition, part of the YY1-mediated metabolic program is controlled in a lineage-specific manner by interaction with lineage-specific co-factors, including MITF and SOX10.

STAR★METHODS

Detailed methods are provided in the online version of this paper and include the following:

- KEY RESOURCES TABLE
- CONTACT FOR REAGENT AND RESOURCE SHARING
- EXPERIMENTAL MODEL AND SUBJECT DETAILS
  - Mice
  - Cell Lines
- METHOD DETAILS
  - Animal Experimentation
  - Isolation of Migratory NC Cells and Priming
  - Isolation of Branchial Arch 1 (BA1) Cells
  - Isolation of Wild-type and Tyr::Nras^{Q61K};Cdkn2a$^{-/-}$ Melanoma Competent Melanocytes from Mouse Skin
  - Alcian Blue Staining
  - Immunohistochemistry
  - Detection of Proliferation and Apoptosis Rates
  - Protein Isolation and Western Blotting
  - RNA Isolation, Microarray, RNA-seq and qRT-PCR
  - ChIP-seq
  - Oxygen Consumption Rate (OCR)
  - Untargeted Metabolomics
  - Exogenous Metabolite Supplementation
  - Protein Synthesis Rates
  - Molecular Cloning
  - Cell Transfections, Viral Production and Viral Transduction of Melanoma Cells
  - Integration of YY1, SOX10 and MITF Binding Sites
- QUANTIFICATION AND STATISTICAL ANALYSIS
- DATA AND SOFTWARE AVAILABILITY

SUPPLEMENTAL INFORMATION

Supplemental Information can be found online at https://doi.org/10.1016/j.stem.2019.03.011.

ACKNOWLEDGMENTS

We thank F. Beermann, M. Serrano, R. Kemler, and L. Dimou for providing *Tyr::Nras*^{Q61k}, *Cdkn2a*$^{-/-}$, *Wnt1::Cre*, and *Sox10::CreER*^{T2} mice, respectively. We thank all former and current laboratory members for their critical input. We thank Annika Klug, Martina Zemke, Simon Schaefer, and Vadims Parfejevs for technical support. S.V. is funded by the Zurich University Research Priority Program "Translational Cancer Research." Z.K.A. and J.W. are funded by postdoctoral research fellowships from Kom op Tegen Kanker. Research in the S.A. laboratory is funded by ERC CoG 724226 - cis-CONTROL. Work in the L.S. laboratory is supported by the Swiss National Science Foundation, the Swiss Cancer League, the Zurich University Research Priority Program "Translational Cancer Research," and the Foundation for Research in Science and Humanities at University of Zurich.

AUTHOR CONTRIBUTIONS

S.V. and L.S. conceived the project and designed the study. S.V., A.B., L.Z., E.M., R.B., J.H., E.T., D.V., N.J., M.B., and N.Z. performed experiments and analyzed data. C.C., Z.K.A., J.W., D.Z., N.Z., S.A., M.P.L., K.B., and R.D. analyzed data and provided intellectual guidance in design of experiments and interpretation of results. S.V. and L.S. wrote the manuscript.

DECLARATION OF INTERESTS

The authors declare no competing interests.

Received: November 29, 2018
Revised: January 29, 2019
Accepted: March 11, 2019
Published: April 4, 2019

REFERENCES

Ackermann, J., Frutschi, M., Kaloulis, K., McKee, T., Trumpp, A., and Beermann, F. (2005). Metastasizing melanoma formation caused by expression of activated N-RasQ61K on an INK4a-deficient background. Cancer Res. *65*, 4005–4011.

Affar, B., Gay, F., Shi, Y., Liu, H., Huarte, M., Wu, S., Collins, T., Li, E., and Shi, Y. (2006). Essential dosage-dependent functions of the transcription factor yin yang 1 in late embryonic development and cell cycle progression. Mol. Cell. Biol. *26*, 3565–3581.

Akbani, R., Akdemir, K.C., Aksoy, B.A., Albert, M., Ally, A., Amin, S.B., Arachchi, H., Arora, A., Auman, J.T., Ayala, B., et al.; Cancer Genome Atlas Network (2015). Genomic classification of cutaneous melanoma. Cell *161*, 1681–1696.

Albers, J., Danzer, C., Rechsteiner, M., Lehmann, H., Brandt, L.P., Hejhal, T., Catalano, A., Busenhart, P., Gonçalves, A.F., Brandt, S., et al. (2015). A versatile modular vector system for rapid combinatorial mammalian genetics. J. Clin. Invest. *125*, 1603–1619.

Baggiolini, A., Varum, S., Mateos, J.M., Bettosini, D., John, N., Bonalli, M., Ziegler, U., Dimou, L., Clevers, H., Furrer, R., and Sommer, L. (2015). Premigratory and migratory neural crest cells are multipotent in vivo. Cell Stem Cell *16*, 314–322.

Balwierz, P.J., Pachkov, M., Arnold, P., Gruber, A.J., Zavolan, M., and van Nimwegen, E. (2014). ISMARA: automated modeling of genomic signals as a democracy of regulatory motifs. Genome Res. *24*, 869–884.

Barna, M., Pusic, A., Zollo, O., Costa, M., Kondrashov, N., Rego, E., Rao, P.H., and Ruggero, D. (2008). Suppression of Myc oncogenic activity by ribosomal protein haploinsufficiency. Nature *456*, 971–975.

Bernhardt, M., Novak, D., Assenov, Y., Orouji, E., Knappe, N., Weina, K., Reith, M., Larribere, L., Gebhardt, C., Plass, C., et al. (2017). Melanoma-derived iPCCs show differential tumorigenicity and therapy response. Stem Cell Reports *8*, 1379–1391.

Blättler, S.M., Verdeguer, F., Liesa, M., Cunningham, J.T., Vogel, R.O., Chim, H., Liu, H., Romanino, K., Shirihai, O.S., Vazquez, F., et al. (2012). Defective mitochondrial morphology and bioenergetic function in mice lacking the transcription factor Yin Yang 1 in skeletal muscle. Mol. Cell. Biol. *32*, 3333–3346.

Bosenberg, M., Muthusamy, V., Curley, D.P., Wang, Z., Hobbs, C., Nelson, B., Nogueira, C., Horner, J.W., 2nd, Depinho, R., and Chin, L. (2006). Characterization of melanocyte-specific inducible Cre recombinase transgenic mice. Genesis *44*, 262–267.

Boumahdi, S., Driessens, G., Lapouge, G., Rorive, S., Nassar, D., Le Mercier, M., Delatte, B., Caauwe, A., Lenglez, S., Nkusi, E., et al. (2014). SOX2 controls tumour initiation and cancer stem-cell functions in squamous-cell carcinoma. Nature *511*, 246–250.

Carreira, S., Goodall, J., Aksan, I., La Rocca, S.A., Galibert, M.-D., Denat, L., Larue, L., and Goding, C.R. (2005). Mitf cooperates with Rb1 and activates p21Cip1 expression to regulate cell cycle progression. Nature *433*, 764–769.

Danielian, P.S., Muccino, D., Rowitch, D.H., Michael, S.K., and McMahon, A.P. (1998). Modification of gene activity in mouse embryos in utero by a tamoxifen-inducible form of Cre recombinase. Curr. Biol. *8*, 1323–1326.

Dubuis, S., Baenke, F., Scherbichler, N., Alexander, L.T., Schulze, A., and Zamboni, N. (2017). Metabotypes of breast cancer cell lines revealed by non-targeted metabolomics. Metab. Eng. *43*, 173–186.

Dupin, E., and Sommer, L. (2012). Neural crest progenitors and stem cells: from early development to adulthood. Dev. Biol. *366*, 83–95.

Falletta, P., Sanchez-Del-Campo, L., Chauhan, J., Effern, M., Kenyon, A., Kershaw, C.J., Siddaway, R., Lisle, R., Freter, R., Daniels, M.J., et al. (2017). Translation reprogramming is an evolutionarily conserved driver of phenotypic plasticity and therapeutic resistance in melanoma. Genes Dev. *31*, 18–33.

Feng, Y., Pinkerton, A.B., Hulea, L., Zhang, T., Davies, M.A., Grotegut, S., Cheli, Y., Yin, H., Lau, E., Kim, H., et al. (2015). SBI-0640756 attenuates the growth of clinically unresponsive melanomas by disrupting the eIF4F translation initiation complex. Cancer Res. *75*, 5211–5218.

Ferguson, J., Smith, M., Zudaire, I., Wellbrock, C., and Arozarena, I. (2017). Glucose availability controls ATF4-mediated MITF suppression to drive melanoma cell growth. Oncotarget *8*, 32946–32959.

Fuchs, S., Herzog, D., Sumara, G., Büchmann-Møller, S., Civenni, G., Wu, X., Chrostek-Grashoff, A., Suter, U., Ricci, R., Relvas, J.B., et al. (2009). Stage-specific control of neural crest stem cell proliferation by the small rho GTPases Cdc42 and Rac1. Cell Stem Cell *4*, 236–247.

Fuhrer, T., Heer, D., Begemann, B., and Zamboni, N. (2011). High-throughput, accurate mass metabolome profiling of cellular extracts by flow injection-time-of-flight mass spectrometry. Anal. Chem. *83*, 7074–7080.

Gabriele, M., Vulto-van Silfhout, A.T., Germain, P.-L., Vitriolo, A., Kumar, R., Douglas, E., Haan, E., Kosaki, K., Takenouchi, T., Rauch, A., et al. (2017). YY1 haploinsufficiency causes an intellectual disability syndrome featuring transcriptional and chromatin dysfunction. Am. J. Hum. Genet. *100*, 907–925.

Greenwood, A.L., Turner, E.E., and Anderson, D.J. (1999). Identification of dividing, determined sensory neuron precursors in the mammalian neural crest. Development *126*, 3545–3559.

Haq, R., Shoag, J., Andreu-Perez, P., Yokoyama, S., Edelman, H., Rowe, G.C., Frederick, D.T., Hurley, A.D., Nellore, A., Kung, A.L., et al. (2013). Oncogenic BRAF regulates oxidative metabolism via PGC1α and MITF. Cancer Cell *23*, 302–315.

Harris, M.L., Buac, K., Shakhova, O., Hakami, R.M., Wegner, M., Sommer, L., and Pavan, W.J. (2013). A dual role for SOX10 in the maintenance of the postnatal melanocyte lineage and the differentiation of melanocyte stem cell progenitors. PLoS Genet. *9*, e1003644.

He, Y., Kim, J.Y., Dupree, J., Tewari, A., Melendez-Vasquez, C., Svaren, J., and Casaccia, P. (2010). Yy1 as a molecular link between neuregulin and transcriptional modulation of peripheral myelination. Nat. Neurosci. *13*, 1472–1480.

Hoek, K.S., Eichhoff, O.M., Schlegel, N.C., Döbbeling, U., Kobert, N., Schaerer, L., Hemmi, S., and Dummer, R. (2008). In vivo switching of human melanoma cells between proliferative and invasive states. Cancer Res. *68*, 650–656.

Hu, J., Locasale, J.W., Bielas, J.H., O'Sullivan, J., Sheahan, K., Cantley, L.C., Vander Heiden, M.G., and Vitkup, D. (2013). Heterogeneity of tumor-induced gene expression changes in the human metabolic network. Nat. Biotechnol. *31*, 522–529.

Imrichová, H., Hulselmans, G., Atak, Z.K., Potier, D., and Aerts, S. (2015). i-cisTarget 2015 update: generalized cis-regulatory enrichment analysis in human, mouse and fly. Nucleic Acids Res. *43* (W1), W57–W64.

John, N., Cinelli, P., Wegner, M., and Sommer, L. (2011). Transforming growth factor β-mediated Sox10 suppression controls mesenchymal progenitor generation in neural crest stem cells. Stem Cells *29*, 689–699.

Kaufman, C.K., Mosimann, C., Fan, Z.P., Yang, S., Thomas, A.J., Ablain, J., Tan, J.L., Fogley, R.D., van Rooijen, E., Hagedorn, E.J., et al. (2016). A zebrafish melanoma model reveals emergence of neural crest identity during melanoma initiation. Science *351*, aad2197.

Kerosuo, L., and Bronner, M.E. (2016). cMyc regulates the size of the premigratory neural crest stem cell pool. Cell Rep. *17*, 2648–2659.

Kleiman, E., Jia, H., Loguercio, S., Su, A.I., and Feeney, A.J. (2016). YY1 plays an essential role at all stages of B-cell differentiation. Proc. Natl. Acad. Sci. USA *113*, E3911–E3920.

Laurette, P., Strub, T., Koludrovic, D., Keime, C., Le Gras, S., Seberg, H., Van Otterloo, E., Imrichova, H., Siddaway, R., Aerts, S., et al. (2015). Transcription factor MITF and remodeller BRG1 define chromatin organisation at regulatory elements in melanoma cells. eLife *4*, e06857.

Leucci, E., Vendramin, R., Spinazzi, M., Laurette, P., Fiers, M., Wouters, J., Radaelli, E., Eyckerman, S., Leonelli, C., Vanderheyden, K., et al. (2016). Melanoma addiction to the long non-coding RNA SAMMSON. Nature *531*, 518–522.

Li, J., Song, J.S., Bell, R.J.A., Tran, T.-N.T., Haq, R., Liu, H., Love, K.T., Langer, R., Anderson, D.G., Larue, L., and Fisher, D.E. (2012). YY1 regulates melanocyte development and function by cooperating with MITF. PLoS Genet. *8*, e1002688.

Lu, L., Sun, K., Chen, X., Zhao, Y., Wang, L., Zhou, L., Sun, H., and Wang, H. (2013). Genome-wide survey by ChIP-seq reveals YY1 regulation of lincRNAs in skeletal myogenesis. EMBO J. *32*, 2575–2588.

Ng, S.B., Buckingham, K.J., Lee, C., Bigham, A.W., Tabor, H.K., Dent, K.M., Huff, C.D., Shannon, P.T., Jabs, E.W., Nickerson, D.A., et al. (2010). Exome sequencing identifies the cause of a mendelian disorder. Nat. Genet. *42*, 30–35.

Perekatt, A.O., Valdez, M.J., Davila, M., Hoffman, A., Bonder, E.M., Gao, N., and Verzi, M.P. (2014). YY1 is indispensable for Lgr5+ intestinal stem cell renewal. Proc. Natl. Acad. Sci. USA *111*, 7695–7700.

Piskounova, E., Agathocleous, M., Murphy, M.M., Hu, Z., Huddlestun, S.E., Zhao, Z., Leitch, A.M., Johnson, T.M., DeBerardinis, R.J., and Morrison, S.J. (2015). Oxidative stress inhibits distant metastasis by human melanoma cells. Nature *527*, 186–191.

Rambow, F., Rogiers, A., Marin-Bejar, O., Aibar, S., Femel, J., Dewaele, M., Karras, P., Brown, D., Chang, Y.H., Debiec-Rychter, M., et al. (2018). Toward minimal residual disease-directed therapy in melanoma. Cell *174*, 843–855.e19.

Ratnikov, B.I., Scott, D.A., Osterman, A.L., Smith, J.W., and Ronai, Z.A. (2017). Metabolic rewiring in melanoma. Oncogene *36*, 147–157.

Ross, A.P., and Zarbalis, K.S. (2014). The emerging roles of ribosome biogenesis in craniofacial development. Front. Physiol. *5*, 26.

Rubinfeld, B., Robbins, P., El-Gamil, M., Albert, I., Porfiri, E., and Polakis, P. (1997). Stabilization of beta-catenin by genetic defects in melanoma cell lines. Science *275*, 1790–1792.

Ruggero, D. (2013). Translational control in cancer etiology. Cold Spring Harb. Perspect. Biol. *5*, a012336.

Schaefer, S.M., Segalada, C., Cheng, P.F., Bonalli, M., Parfejevs, V., Levesque, M.P., Dummer, R., Nicolis, S.K., and Sommer, L. (2017). Sox2 is dispensable for primary melanoma and metastasis formation. Oncogene *36*, 4516–4524.

Serrano, M., Lee, H., Chin, L., Cordon-Cardo, C., Beach, D., and DePinho, R.A. (1996). Role of the INK4a locus in tumor suppression and cell mortality. Cell *85*, 27–37.

Shakhova, O., Zingg, D., Schaefer, S.M., Hari, L., Civenni, G., Blunschi, J., Claudinot, S., Okoniewski, M., Beermann, F., Mihic-Probst, D., et al. (2012). Sox10 promotes the formation and maintenance of giant congenital naevi and melanoma. Nat. Cell Biol. *14*, 882–890.

Signer, R.A.J., Magee, J.A., Salic, A., and Morrison, S.J. (2014). Haematopoietic stem cells require a highly regulated protein synthesis rate. Nature *509*, 49–54.

Simões-Costa, M., Tan-Cabugao, J., Antoshechkin, I., Sauka-Spengler, T., and Bronner, M.E. (2014). Transcriptome analysis reveals novel players in the cranial neural crest gene regulatory network. Genome Res. *24*, 281–290.

Simon, C., Lickert, H., Götz, M., and Dimou, L. (2012). Sox10-iCreERT2 : a mouse line to inducibly trace the neural crest and oligodendrocyte lineage. Genesis *50*, 506–515.

Singleton, K.R., Crawford, L., Tsui, E., Manchester, H.E., Maertens, O., Liu, X., Liberti, M.V., Magpusao, A.N., Stein, E.M., Tingley, J.P., et al. (2017). Melanoma therapeutic strategies that select against resistance by exploiting MYC-driven evolutionary convergence. Cell Rep. *21*, 2796–2812.

Stine, Z.E., Walton, Z.E., Altman, B.J., Hsieh, A.L., and Dang, C.V. (2015). MYC, metabolism, and cancer. Cancer Discov. *5*, 1024–1039.

Strub, T., Giuliano, S., Ye, T., Bonet, C., Keime, C., Kobi, D., Le Gras, S., Cormont, M., Ballotti, R., Bertolotto, C., and Davidson, I. (2011). Essential role of microphthalmia transcription factor for DNA replication, mitosis and genomic stability in melanoma. Oncogene *30*, 2319–2332.

Suvà, M.L., Riggi, N., and Bernstein, B.E. (2013). Epigenetic reprogramming in cancer. Science *339*, 1567–1570.

Suvà, M.L., Rheinbay, E., Gillespie, S.M., Patel, A.P., Wakimoto, H., Rabkin, S.D., Riggi, N., Chi, A.S., Cahill, D.P., Nahed, B.V., et al. (2014). Reconstructing and reprogramming the tumor-propagating potential of glioblastoma stem-like cells. Cell *157*, 580–594.

Vander Heiden, M.G., and DeBerardinis, R.J. (2017). Understanding the intersections between metabolism and cancer biology. Cell *168*, 657–669.

Varum, S., Rodrigues, A.S., Moura, M.B., Momcilovic, O., Easley, C.A., 4th, Ramalho-Santos, J., Van Houten, B., and Schatten, G. (2011). Energy metabolism in human pluripotent stem cells and their differentiated counterparts. PLoS ONE *6*, e20914.

Vazquez, F., Lim, J.-H., Chim, H., Bhalla, K., Girnun, G., Pierce, K., Clish, C.B., Granter, S.R., Widlund, H.R., Spiegelman, B.M., and Puigserver, P. (2013). PGC1α expression defines a subset of human melanoma tumors with increased mitochondrial capacity and resistance to oxidative stress. Cancer Cell *23*, 287–301.

Vendramin, R., Verheyden, Y., Ishikawa, H., Goedert, L., Nicolas, E., Saraf, K., Armaos, A., Delli Ponti, R., Izumikawa, K., Mestdagh, P., et al. (2018). SAMMSON fosters cancer cell fitness by concertedly enhancing mitochondrial and cytosolic translation. Nat. Struct. Mol. Biol. *25*, 1035–1046.

Weintraub, A.S., Li, C.H., Zamudio, A.V., Sigova, A.A., Hannett, N.M., Day, D.S., Abraham, B.J., Cohen, M.A., Nabet, B., Buckley, D.L., et al. (2017). YY1 is a structural regulator of enhancer-promoter loops. Cell *171*, 1573–1588.e28.

White, R.M., Cech, J., Ratanasirintrawoot, S., Lin, C.Y., Rahl, P.B., Burke, C.J., Langdon, E., Tomlinson, M.L., Mosher, J., Kaufman, C., et al. (2011). DHODH modulates transcriptional elongation in the neural crest and melanoma. Nature *471*, 518–522.

Wilcox, A.J., Lie, R.T., Solvoll, K., Taylor, J., McConnaughey, D.R., Abyholm, F., Vindenes, H., Vollset, S.E., and Drevon, C.A. (2007). Folic acid supplements and risk of facial clefts: national population based case-control study. BMJ *334*, 464.

Zeller, K.I., Zhao, X., Lee, C.W.H., Chiu, K.P., Yao, F., Yustein, J.T., Ooi, H.S., Orlov, Y.L., Shahab, A., Yong, H.C., et al. (2006). Global mapping of c-Myc binding sites and target gene networks in human B cells. Proc. Natl. Acad. Sci. USA *103*, 17834–17839.

Zingg, D., Debbache, J., Schaefer, S.M., Tuncer, E., Frommel, S.C., Cheng, P., Arenas-Ramirez, N., Haeusel, J., Zhang, Y., Bonalli, M., et al. (2015). The epigenetic modifier EZH2 controls melanoma growth and metastasis through silencing of distinct tumour suppressors. Nat. Commun. *6*, 6051.

STAR★METHODS

KEY RESOURCES TABLE

REAGENT or RESOURCE	SOURCE	IDENTIFIER
Antibodies		
Goat anti-Sox10 Polyclonal Antibody	Santa Cruz Biotechnology	Cat# sc-17342; RRID:AB_2195374
Goat anti-Sox9 Polyclonal Antibody	Santa Cruz Biotechnology	Cat# sc-20095; RRID:AB_661282
Mouse anti-NF160 Monoclonal Antibody	Sigma-Aldrich	Cat# N-5264; RRID:AB_477278
Rabbit anti-Fabp7 Polyclonal Antibody	Abcam	Cat# ab32423; RRID:AB_880078
Goat anti-Dct Polyclonal Antibody	Santa Cruz Biotechnology	Cat# sc-10451; RRID:AB_793582
Rabbit anti-cleaved Caspase 3 Polyclonal Antibody	Cell Signaling Technology	Cat# 9661
Rabbit anti-YY1 (H-414) Polyclonal Antibody	Santa Cruz Biotechnology	Cat# sc-1703; RRID:AB_2218501
Rabbit anti-YY1 (D5D9Z) Polyclonal Antibody	Cell Signaling Technology	Cat# 46395
Rabbit anti-RFP Polyclonal Antibody	Rockland	Cat# 600-401-379; RRID:AB_2209751
Goat anti-tdTomato Polyclonal Antibody	LifeSpan BioSciences	Cat# LS-C340696
Chicken anti-GFP Polyclonal Antibody	Aves Labs	Cat# GFP-1020; RRID:AB_10000240
Mouse anti-α Tubulin Monoclonal Antibody	Sigma-Aldrich	Cat# T6074; RRID:AB_477582
Rabbit anti-IgG	Santa Cruz Biotechnology	Cat# sc-2027; RRID:AB_737197
Mouse anti-MITF (C5) Monoclonal Antibody	Abcam	Cat# ab12039; RRID:AB_298801
Rat anti-cKit-APC Conjugated Monoclonal Antibody	Thermo Fischer Scientific	Cat# 17-1171-81; RRID:AB_469429
Goat anti-Mouse IgG (H+L) Alexa Fluor 488	Thermo Fischer Scientific	Cat# A-11029; RRID:AB_138404
Goat anti-Rabbit IgG (H+L) Cy3	Jackson ImmunoResearch	111-165-003; RRID:AB_2338000
Donkey anti-Goat IgG (H+L) Alexa Fluor 647	Jackson ImmunoResearch	Cat# 705-605-147; RRID:AB_2340437
Donkey anti-Chicken IgY (H+L) Cy3	Jackson ImmunoResearch	Cat# 703-165-155; RRID:AB_2340363
Donkey anti-Goat IgG (H+L) Cy3	Jackson ImmunoResearch	Cat# 705-165-147; RRID:AB_2307351
Donkey anti-Rabbit IgG (H+L) Cy3	Jackson ImmunoResearch	Cat# 711-165-152; RRID:AB_2307443
Donkey anti-Mouse IgG (H+L) Cy3	Jackson ImmunoResearch	Cat# 715-165-150; RRID:AB_2340813
Donkey anti-Rabbit IgG (H+L) Alexa Fluor 488	Jackson ImmunoResearch	Cat# 711-545-152; RRID:AB_2313584
Donkey anti-Mouse IgG (H+L) Alexa Fluor 488	Jackson ImmunoResearch	Cat# 715-545-150; RRID:AB_2340846
Donkey anti-Goat IgG (H+L) Biotin-Streptavidin	Jackson ImmunoResearch	Cat# 705-065-003; RRID:AB_2340396
Peroxidase Streptavidin	Jackson ImmunoResearch	Cat# 016-030-084; RRID:AB_2337238
Donkey anti-Mouse IgG IRdye 800 CW	Li-COR Biosciences	Cat# 926-32212; RRID:AB_621847
Donkey anti-Rabbit IgG, IRdye 680LT	Li-COR Biosciences	Cat# 926-68023; RRID:AB_10706167
Donkey anti-Mouse IgG IRdye 680LT	Li-COR Biosciences	Cat# 926-68022; RRID:AB_10715072
Bacterial and Virus Strains		
One Shot Stbl3 Chemically Competent *E. coli*	Thermo Fischer Scientific	Cat# C737303
Lentiviral-cMYC-EGFP	This paper	N/A
Lentiviral-EGFP	This paper	N/A
Adenoviral-Ad-H1-Si-MITF	Gift from M. Levesque's Lab (Hoek et al., 2008)	N/A
Adenoviral-Ad-H1-Si-Control	Gift from M. Levesque's Lab (Hoek et al., 2008)	N/A
Biological Samples		
Wnt1::Cre Embryos: *Wnt1::Cre;Yy1*$^{fl/wt}$; *Wnt1::Cre;Yy1*$^{fl/fl}$; *Wnt1::Cre;Yy1*$^{wt/wt}$	This paper	N/A
Sox10::CreER^{T2} Embryos: *Sox10::CreER*^{T2}*;Yy1*$^{fl/wt}$; *Sox10::CreER*^{T2}*;Yy1*$^{fl/fl}$; *Sox10::CreER*^{T2}*Cre;Yy1*$^{wt/wt}$	This paper	N/A
Wild type skin sections: *Tyr::CreER*^{T2}*;Yy1*$^{fl/wt}$; *Tyr::CreER*^{T2}*;Yy1*$^{fl/fl}$; *Tyr::CreER*^{T2}*;Yy1*$^{wt/wt}$	This paper	N/A

(*Continued on next page*)

Continued

REAGENT or RESOURCE	SOURCE	IDENTIFIER
Skin sections from *Tyr::Nras^{Q61K};Cdkn2a$^{-/-}$: Tyr::CreER^{T2};Yy1$^{fl/wt}$; Tyr::CreER^{T2};Yy1$^{fl/fl}$; Tyr::CreER^{T2};Yy1$^{wt/wt}$*	This paper	N/A
Melanocytes from wild type and *Tyr::Nras^{Q61K};Cdkn2a$^{-/-}$* animals	This paper	N/A
RIM melanomas from: *Tyr::Nras^{Q61K};Cdkn2a$^{-/-}$; Tyr::CreER^{T2};Yy1$^{fl/wt}$*	This paper	N/A
Human melanoma cell cultures	URPP Live Biobank, University of Zurich	N/A
BA1 cells from: *Wnt1::Cre;Yy1$^{fl/wt}$; Wnt1::Cre;Yy1$^{fl/fl}$; Wnt1::Cre;Yy1$^{wt/wt}$*	This paper	N/A
Chemicals, Peptides, and Recombinant Proteins		
FCS	Thermo Fischer Scientific	Cat# 16140
L-glutamine	Thermo Fischer Scientific	Cat# 25030
Tamoxifen	Sigma-Aldrich	Cat# T5648; CAS# 10540-29-1
Isoflurane	Piramal Healthcare	Cat# 430024079
Fibronectin	Sigma-Aldrich	Cat# F11141
Human Recombinant TGFβ1	PrepoTech	Cat# 100-21
Human Recombinant BMP2	PrepoTech	Cat# 120-02
Human Recombinant Neuregulin Type I	PrepoTech	Cat#100-03
Fibronectin	Sigma-Aldrich	Cat# F6886; CAS# 66575-29-9
HBSS (no Calcium or Magnesium)	Thermo Fischer Scientific	Cat# 14170
Collagenase Type 3	Worthington	Cat# M3D14157
Trypsin	Thermo Fischer Scientific	Cat# 25200
B27 Supplement	Thermo Fischer Scientific	Cat# 12587-010
N2 Supplement	Thermo Fischer Scientific	Cat# 17502-048
FGF2	R&D Systems	Cat# 233-FB-001MG/CF
CHIR 99021	Tocris	Cat# 44230
Liberase DH Research Grade	Roche	Cat# 0.5401054001
DNAase I	Roche	Cat# 10104159001
RLT Buffer	QIAGEN	Cat# 79216
Bouin's Fixative	Sigma-Aldrich	Cat# HT101128
Ammonium Hydroxide	Sigma-Aldrich	Cat# 338818; CAS#1336-21-6
Alcian Blue	Sigma-Aldrich	Cat# A5268; CAS# 33864-99-2
Acetic Acid	Sigma-Aldrich	Cat# A6283; CAS# 64-19-7
Benzyl Alcohol	Sigma-Aldrich	Cat# 305197; CAS# 100-51-6
Benzyl Benzoate	Sigma-Aldrich	Cat# B6630; CAS# 120-51-4
O.C.T Compound	Scigen	Cat# AGR1180
Roti-Histofix	Carl Roth	Cat# P087.3
Tween-20	Sigma-Aldrich	Cat# P1379; CAS# 9005-64-5
Blocking Reagent	Perkin-Elmer	Cat# FP1020
Hoeschst 33342	Sigma-Aldrich	Cat# 14533; CAS# 23491-52-3
Fluorescent Mounting Medium	Dako	Cat# S3023
EdU	Thermo Fischer Scientific	Cat# C10424
RIPA Buffer	Thermo Fischer Scientific	Cat# 89900
Protease Inhibitor	Thermo Fischer Scientific	Cat# 87786
Phosphatase Inhibitor	Thermo Fischer Scientific	Cat# 78420
Odyssey Blocking Buffer	Li-COR Biosciences	Odyssey blocking buffer
SYBR Green I Master Mix	Roche	Cat# 4707516001
Non-buffered XF Base DMEM Minimal Medium	Agilent	Cat# 103334

(*Continued on next page*)

Continued

REAGENT or RESOURCE	SOURCE	IDENTIFIER
Oligomycin	Agilent	Cat# 103015-100
Acetonitrile	Sigma-Aldrich	Cat# 271004; CAS# 75-05-8
Uridine	Sigma-Aldrich	Cat# U3003; CAS# 58-96-8
Glutamic Acid Dimethyl Ester	Sigma-Aldrich	Cat# 49560; CAS# 23150-65-4
L-aspartic Acid Dimethyl Ester	Sigma-Aldrich	Cat# 456233; CAS# 32213-95-9
L-Carnitine Hydrochloride	Sigma-Aldrich	Cat# 456233; CAS# 32213-95-9
Nucleoside Mix	Millipore	Cat# ES-008-D
OP-Puro	Jena Bioscience	Cat# Nu-931-5
PI/RNase Solution	Invitrogen	Cat# F10797
Polybrene	Sigma-Aldrich	Cat# H9268; CAS# 28728-55-4
FCCP	Agilent	Cat# 103015-100
Antimycin/Rotenone	Agilent	Cat# 103015-100
Dispase I	Roche	Cat# 04942086001
Critical Commercial Assays		
Annexin V Apoptosis Detection Kit	BD PharMingen	Cat# 556547
Click-iT EdU Alexa Fluor 647 Flow Cytometry Assay Kit	Thermo Fischer Scientific	Cat# C10424
TSA Plus Cyanine System	Perkin-Elmer	Cat# NEL744001
Maxima First Strand cDNA Synthesis kit	Thermo Fischer Scientific	Cat# K1641
Magna ChIP A/G kit	Millipore	Cat# 17-10085/86
Seahorse Mito Stress Test kit	Agilent	Cat# 103015-100
High Fidelity PCR Master Kit	Roche	Cat# 2140314001
Anza T4 DNA Ligase Master Mix	Thermo Fischer Scientific	Cat# IVGN2108
Gateway LR Clonase II mix	Thermo Fischer Scientific	Cat# 11791020
Click-IT Protein Synthesis Assay Kit	Thermo Fischer Scientific	Cat# C10458
Jet Prime Transfection Reagent	Polyplus	Cat# 114-75
RNAeasy Mini Kit	QIAGEN	Cat# 74106
QIAquick Gel Extraction Kit	QIAGEN	Cat# 28704
Deposited Data		
RNa-seq in Control and *Yy1* cko BA1 cells	This paper	PRJEB21547
RNA-seq in Si-Control and Si-YY1 human melanoma cells	This paper	PRJEB21636
YY1 ChIP seq	This paper	PRJEB21646
MITF ChiP seq	(Strub et al., 2011)	GSM1565011
SOX10 ChIP seq	(Laurette et al., 2015)	GSM1517752
RNA-seq in wild-type melanocytes and $Nras^{Q61K}$;$Cdkn2a^{-/-}$ melanocytes	This paper	PRJEB30285
Microarray in NCSCs and their primed counterparts	This paper	GEO: GSE125480
Experimental Models: Cell Lines		
Human Melanoma: M010817	URPP Live Cell Biobank, University of Zurich	N/A
Human Melanoma: M050829	URPP Live Cell Biobank, University of Zurich	N/A
Human Melanoma: M980513	URPP Live Cell Biobank, University of Zurich	N/A
Human Melanoma: M000921	URPP Live Cell Biobank, University of Zurich	N/A
Human Melanoma: M130429	URPP Live Cell Biobank, University of Zurich	N/A
Human Melanoma: Skmel28	ATCC	Cat# HBT-72
Human Melanoma: A375	ATCC	Cat# CRL-1619
Human Melanoma: Mel888	(Rubinfeld et al., 1997)	N/A

(*Continued on next page*)

Continued

REAGENT or RESOURCE	SOURCE	IDENTIFIER
Human Prostate Cancer: PC3	ATCC	Cat# CRL-1435
Human Prostate Cancer: Du145	ATCC	Cat# HTB-81
Human Breast Cancer: MDA-MB-231	ATCC	Cat# HTB26
Human Breast Cancer: T47-D	ATCC	Cat# HBT-133
Human Colon Cancer: WIDr	ATCC	Cat# CCL-218
Human Adrenal Carcinoma: NCI-H295R	ATCC	Cat# CRL-2128
HEK293T	ATCC	Cat# CRL-1573
Experimental Models: Organisms/Strains		
Mouse *Wnt1::Cre*: H2afv$^{Tg(Wnt1\text{-}cre)11Rth}$	(Danielian et al., 1998)	MGI: 2386570
Mouse *Sox10::CreER^{T2}:* Tg(Sox10-icre/ERT2)1Ldim	(Simon et al., 2012)	N/A
Mouse: Hsd:Athymic Nude-Foxn1$^{nu/nu}$	Envigo	N/A
Mouse: *Tyr::CreER^{T2}*: B6.Cg-Tg(Tyr-cre/ERT2)13Bos/J	The Jackson Laboratory	Cat# 012328; RRID: IMSR_JAX:012328
Mouse: R26R-LSL-tdTomato: B6.Cg-Gt(ROSA) 26Sortm14(CAG-tdTomato)Hze/J	The Jackson Laboratory	Cat# 007914; RRID: IMSR_JAX:007914
Mouse:*Yy1$^{fl/fl}$*: B6;129S4-Yy1tm2Yshi/J	The Jackson Laboratory	Cat# 014649; RRID:IMSR_JAX:014649
Mouse: R26R-EGFP: Gt(ROSA)26Sortm1Sho	The Jackson Laboratory	Cat# 003504; RRID:IMSR_JAX:003504
Oligonucleotides		
Mouse Genotype Primers, See Table S5	Mycrosynth	N/A
Human qRT-PCR Primers, See Table S6	Mycrosynth	N/A
Mouse qRT-PCR Primers, See Table S6	Mycrosynth	N/A
Mouse ChiP qRT-PCR Primers, See Table S7	Mycrosynth	N/A
Recombinant DNA		
Stealth Si RNA Targeting YY1 (Si-YY1)	Thermo Fischer Scientific	Cat# YY1HSS111432
Stealth Medium GC Content Scrambled Si RNA (Si-Control)	Thermo Fischer Scientific	Cat# 12935
pCDH-Puro-cMYC	Addgene	Cat# 46970
pMuLE-ENTR-CMV-L1-R5 Vector	Addgene (Albers et al., 2015)	Cat# 62090
pMuLE-ENTR-SV40-eGFP-L5-L2	Addgene (Albers et al., 2015)	Cat# 62144
pLenti-X1-Piro-DEST	Addgene (Albers et al., 2015)	Cat# 11297
Software and Algorithms		
UCSC Genome Browser	https://genome.uscs.edu/	N/A
Human Metabolome Database v3.0	http://www.hmdb.ca/	N/A
Small Molecule Pathway Database	http://smpdb.ca/	N/A
MACS Software	http://liulab.dfci.harvard.edu/MACS/	N/A
SeqMINER	http://bips.u-strasbg.fr/seqminer/	N/A
ISMARA	https://ismara.unibas.ch /mara	N/A
ClueGo v2.3.2	http://apps.cytoscape.org/apps/cluego	N/A
Cytoscape v3.4.0	https://cytoscape.org	N/A
Graphpad Prism	GraphPad	N/A
MATLAB	https://ch.mathworks.com	N/A
FlowJo v7.6	Tree Star	N/A
Bowtie 2	http://bowtie-bio.sourceforge.net/bowtie2/index.shtml	N/A
HOMER tool package	http://homer.ucsd.edu/homer/	N/A

CONTACT FOR REAGENT AND RESOURCE SHARING

Additional information and requests for reagents may be directed to and will be fulfilled by the Lead Contact, Lukas Sommer (lukas.sommer@anatomy.uzh.ch).

EXPERIMENTAL MODEL AND SUBJECT DETAILS

Mice

Mice carrying the transgenic alleles: *Tyr::CreER^{T2}*, *Yy1$^{fl/fl}$*, *R26R-LSL-tdTomato*, and *R26R-EGFP* were derived from Jackson laboratories. Mice carrying the transgenic alleles: *Wnt1::Cre* (Danielian et al., 1998); *Sox10::CreER^{T2}* (Simon et al., 2012); *Tyr::Nras^{Q61K}* (Ackermann et al., 2005), and mice deficient for *Cdkn2a* (Serrano et al., 1996) were gifts from Rofler Kemler (University of Freiburg), Leda Dimou (University of Ulm, Germany); Friedrich Beermann (Swiss Federal Institute of Technology Lausanne, Switzerland) and Manuel Serrano (Centro Nacional de Investigaciones Oncologicas, Spain), respectively. Mice were bred and crossed in-house to generate the various genotypes described in this paper. Genetic background of experimental animals was mixed and both genders were used. No statistical methods were used to predetermine sample size. All animal breeding, housing and experimentation was conducted according the veterinary office of the Canton of Zurich, Switzerland guidelines. Specifically animals were housed in a controlled environment with a 12- hour light/dark cycle, with free access to water and food.

Cell Lines

Human melanoma cell lines used in this study were: M010817, M050829, M980513, M000921, M130429 (established by URPP Live Cell Biobank, University of Zurich), Skmel28 (Cat#HBT-72, ATCC), A375 (Cat#CRL-1619, ATCC) and Mel888 (Rubinfeld et al., 1997). All melanoma cell lines established at the URPP Live Cell Biobank, University of Zurich were derived with patient consent and according to the Declaration of Helsinki on Human Rights, and approved by the Institutional Review Board (IRB) of Zurich (EK.647/800). All research on surplus human material was conducted under the IRB approval KEK-Zh.Nr 2014-0425. Other cancer cell lines used in this study were PC3 and Du 145 (prostate cancer Cat#CRL-1435 and Cat#HTB-81, respectively), MDA-MB-231 and T-47D (Breast cancer Cat#HTB26 and Cat#HBT-133, respectively), WIDr (colon cancer Cat#CCL-218) and NCI-H295R (Adrenal carcinoma Cat#CRL-2128) all from ATCC. All cell lines were maintained in RPMI 1640 medium (Cat#42401042, Thermo Fischer Scientific) containing 10% FCS (16140, Thermo Fischer Scientific), 4mM L-glutamine (Cat#25030, Thermo Fischer Scientific) and 1% penicillin-streptomycin (Cat#15070, Thermo Fischer Scientific). HEK293T (Cat#CRL-1573) cells were maintained in DMEM (Cat#41965062, Thermo Fischer Scientific) containing 10% FCS and 1% penicillin-streptomycin. Cell lines were maintained at 37°C and 5% C02.

METHOD DETAILS

Animal Experimentation

Timed- matings were performed overnight, by crossing *Wnt1::Cre;Yy1$^{fl/wt}$* mice with *Yy1$^{fl/fl}$* animals. Noon of next day was considered E0.5. *Wnt1::Cre;Yy1$^{fl/fl}$* embryos (here termed *Yy1* cko embryos) were compared with their respective littermates having either no *Wnt1::Cre* transgene (*Yy1$^{fl/wt}$* or *Yy1$^{fl/fl}$*) or lacking a second copy of the floxed Yy1 transgene (*Wnt1::Cre;Yy1$^{fl/wt}$*). To conditionally deplete *Yy1* in post-migratory NC cells, homozygous mice for *Yy1* floxed allele were crossed with *Sox10::CreER^{T2}* mice. Timed-matings were performed as described above. Depletion of *Yy1* in post-migratory NC cells was achieved by injecting either E10.5 or E11.5 pregnant females with a single dose (240 μg/g body weight) of tamoxifen (TM) (Cat#T5648, Sigma-Aldrich) intraperitoneally. *Sox10::CreER^{T2};Yy1$^{fl/fl}$* embryos were compared with respective littermates having either no *Sox10::CreER^{T2}* transgene or lacking a second copy of *Yy1* floxed allele.

To study the role of Yy1 in the adult melanocytic lineage we took advantage of the TM-inducible Cre line *Tyr::CreER^{T2}* (Bosenberg et al., 2006). Transgenic lines were crossed with the *ROSA26* reporter strain expressing *tdTomato*. Depletion of one *Yy1* allele (*Yy1$^{+/-}$*) or two *Yy1* alleles (*Yy1$^{-/-}$*) was induced by 5 consecutive intraperitoneal TM injections (80 μg TM/g body weight-each). To stimulate hair cycle progression, animals were anaesthetized with isoflurane (Cat#430024079, Piramal Healthcare) and dorsal skin was depilated using wax strips (I am, Migros). The first hair plucking was performed at 6 weeks of age and serially repeated approximately every 23 days for 2 times. Mice were sacrificed 9 days after the last hair plucking in order to analyze anagen hair follicles.

To study melanoma initiation we took advantage of the spontaneous melanoma mouse model *Tyr::Nras^{Q61k};Cdkn2a$^{-/-}$*. Conditional depletion of *Yy1* in the melanocytic lineage was achieved by employing the TM-inducible *Tyr::CreER^{T2}* line (Bosenberg et al., 2006). Transgenic lines were crossed with the *ROSA26* reporter strain expressing EGFP. Depletion of one *Yy1* allele or two *Yy1* alleles was induced by 5 consecutive intraperitoneal TM injections (80 μg TM/g body weight-each) at one moth of age. The experimental group included: TM-injected animals expressing the *Tyr::CreER^{T2}* transgene and that contained either one *Yy1* floxed allele (*Tyr::CreER^{T2};Yy1$^{fl/wt}$;R26R-EGFP Tyr::Nras^{Q61K};Cdkn2a$^{-/-}$*) or two *Yy1* floxed alleles (*Tyr::CreER^{T2};Yy1$^{fl/fl}$;R26R-EGFP; Tyr::Nras^{Q61K};Cdkn2a$^{-/-}$*). The control groups included both TM injected animals that lacked the *Tyr::CreER^{T2}* transgene or animals that were not injected with TM. Mice were sacrificed at an endpoint defined by adverse clinical symptoms including tumor size (tumor > 2mm), weight loss or hunched back. Genotyping was performed using primers listed in Table S5. Allografting of murine melanoma cells in athymic nude-Foxn1 mice (Hsd: Athymic nude-*Foxn1$^{nu/nu}$*; Envigo) was performed as previously described (Zingg et al., 2015). Briefly, immunocompromised nude mice were subcutaneously engrafted with melanoma cells derived from *Tyr::CreER^{T2};Yy1$^{fl/wt}$;R26R-EGFP; Tyr::Nras^{Q61K}; Cdkn2a$^{-/-}$* tumors. Nude mice were sacrificed when tumors reached approximately 1,500 mm^3. Tumor material was subsequently engrafted in 10 athymic nude-Foxn1 recipients. Loss of one *Yy1* allele was

induced by 5 consecutive intraperitoneal TM injections (80 μg TM/g body weight-each) when tumors were fully developed. Mice were sacrificed 5 days later and tumor material was further processed.

Isolation of Migratory NC Cells and Priming

Isolation of migratory NC cells was performed as previously described (Greenwood et al., 1999). In brief, E8.75 mouse neural tubes were mechanically isolated, somites were digested with Dispase I (Cat#04942086001, Roche), and neural tubes were plated on fibronectin (Cat#F1141, Sigma-Aldrich). NC cells were allowed to delaminate and migrate out during 20 hours. Priming of NC into the various lineages was achieved by the use of instructing growth factors at the following concentrations: TGFβ1 1ng/ml (Cat#100-21); BMP2 50ng/ml (Cat#120-02), Neuregulin type I 50 μg/ml (Cat#100-03) all from PeproTech, and Forskolin 5 μM (Cat#F6886, Sigma-Aldrich) for mesenchyme, neuronal, and glial fates, respectively. To determine potential transcription factors required for NCSC maintenance we performed a motif activity response analysis by using ISMARA (https://ismara.unibas.ch/fcgi/mara) (Balwierz et al., 2014).

Isolation of Branchial Arch 1 (BA1) Cells

BA1 were mechanically isolated and digested in HBSS without calcium or magnesium (Cat#14170, Thermo Fischer Scientific) containing 0.35mg/ml collagenase type 3 (Cat#M3D14157, Worthington) and 0.04% Trypsin (Cat#25200, Thermo Fischer Scientific). Digestion mix was inactivated, cells were plated in BA1 maintenance medium: Neurobasal medium (Cat#12348-017, Thermo Fischer Scientific) containing 2% B27 supplement (Cat# 12587-010,Thermo Fischer Scientific), 1% N2 supplement (Cat# 17502-048, Thermo Fischer Scientific), 1% L-glutamine (Cat#25030, Thermo Fischer Scientific), 10ng/ml FGF2 (Cat# 233-FB-001MG/CF, R&D Systems) and 1.5 μM of CHIR 99021 (Cat# 44230, Tocris) and kept at 37°C and 5% $C0_2$.

Isolation of Wild-type and Tyr::Nras^{Q61K};Cdkn2a$^{-/-}$ Melanoma Competent Melanocytes from Mouse Skin

Four months old *Tyr::CreER^{T2};R26R-LSL-tdTomato* and *Tyr::Nras^{Q61K};Cdkn2a$^{-/-}$;Tyr::CreER^{T2};R26R-LSL-tdTomato* mice were injected IP with TM for 5 consecutive days (80 μg TM/g body weight-each). Hair cycle growth synchronization in wild-type animals was achieved by dorsal hair plucking (as described above), followed by animal sacrifice 9 days later when anagen hair follicles could be found. Skin was dissociated into small pieces by mechanical dissociation. Digestion was performed by treatment with 0.25mg/ml Liberase DH Research grade (Cat#0.5401054001, Roche) in RPMI 1640 (Cat#42401, Life Technologies) for 1 hour at 37°C, followed by 0.2mg/ml DNAase I (Cat#10104159001, Roche) treatment for 20 minutes at 37°C. Digestion mix was inactivated with RPMI medium containing 10% FCS (Cat#16140, Thermo Fischer Scientific). Cell suspension was filtered through a Falcon cell strainer (Cat#352340, Thermo Fischer Scientific) and centrifuged. Cells were resuspended in RPMI containing 2% FCS incubated for 15 min on ice, followed by incubation with rat anti-cKit conjugated antibody (Cat#17-1171-81, eBisocience; 1:100) in RPMI containing 2% FCS for 30 minutes at room temperature. A washing step was performed with RPMI containing 2% FCS. cKit$^+$ tdTomato$^+$ cells were isolated with a BD FACSAria III Cell Sorter (BD Biosciences) equipped with a 100 um nozzle. Cells were collected into 1.5ml Protein LoBind tubes (Cat#0030108116, Eppendorf) containing RLT buffer (Cat#79216, QIAGEN) and 1% 2-mercaptoethanol (Cat#M3148, Sigma-Aldrich).

Alcian Blue Staining

E14.0 Control and *Yy1* cko embryos were fixed in Bouin's fixative (Cat#HT101128, Sigma-Aldrich) for 2 hours. Embryos were then washed with a 1:1 solution of 0.1% ammonium hydroxide (Cat#338818, Sigma-Aldrich) and 70% ethanol (Cat#51976, Sigma-Aldrich) for 24 hours until embryos loss the yellow coloration. Alcian blue staining was performed with 0.05% Alcian blue (Cat#A5268, Sigma-Aldrich) in 5% acetic acid (Cat#A6283, Sigma-Aldrich) for 2-4 hours. Embryos were washed twice with 5% acetic acid for 1 hour each. Clearing was performed in glass containers by first washing embryos twice in methanol (Cat#34860, Sigma-Aldrich)-2 hours each, and then, by treatment with a 1:2 solution of benzyl alcohol (Cat#305197, Sigma-Aldrich): benzyl benzoate (Cat#B6630, Sigma-Aldrich). Embryos were kept in this solution until imaging.

Immunohistochemistry

Embryos were fixed in 3.7% formaldehyde (Cat#F8775; Sigma-Aldrich) solution in PBS (Cat#10010; Thermo Fischer Scientific) at room temperature for 30 minutes, 2 hours, 3.5 hours and overnight at 4°C for E9.5, E11.5, E13.5 and E14.5, respectively. Embryos were dehydrated in 30% sucrose (Cat#S7903, Sigma-Aldrich) overnight, embedded in O.C.T compound (Cat#AGR1180, Scigen) and stored at −80°C until sectioning into 12 μm cryo-sections. Mouse skin was fixed in 4% Roti-Histofix (Cat#P087.3, Carl Roth) overnight at 4°C, embedded in paraffin and sectioned into 5 μm sections. Deparaffinization was performed as previously described (Zingg et al., 2015). For immunohistochemistry, sections were blocked one hour at room temperature in blocking buffer containing 1% BSA (Cat#05470, Sigma-Aldrich); 0.2% Tween (Cat#P1379, Sigma-Aldrich) in PBS. For Sox10, Sox9, Dct and GFP stainings the blocking buffer used was TNTB buffer (10mM Tris-HCL+ 150mM Nacl + 0.5% blocking reagent, Perkin-Elmer Cat#FP1020). Primary antibodies used were: goat anti-Sox10 (Cat# sc-17342; Santa Cruz Biotechnology; 1:100), rabbit anti-Sox9 (Cat#sc-20095, Santa Cruz Biotechnology; 1:100); mouse anti-NF (Cat#Ab1987, Chemicon; 1:200); rabbit anti-Fabp7 (Cat#ab32423, Abcam; 1:100); goat anti-Dct (Cat#sc-10451; Santa Cruz Biotechnology; 1:100); rabbit anti-cleaved caspase 3 (Cat#9661, Cell Signaling Technology; 1:200); rabbit anti-Yy1(H-414) (Cat#sc-1703, Santa Cruz Biotechnology; 1:100); rabbit anti-Yy1(D5D9Z) (Cat#46395, Cell Signaling Technology; 1:100); rabbit anti-RFP (Cat#600-401-379, Rockland, 1:400); goat anti-tdTomato (Cat#LS-C340696; LifeSpan

BioSciences;1:400); chicken anti-GFP (Cat#1020; Aves, 1:400) and rabbit anti-Brn3a (gift from E. Turner's laboratory). Antibodies were diluted in blocking buffer and incubated overnight at 4°C. Secondary antibodies used were: goat anti-mouse IgG (H+L) Alexa Fluor 488 (Cat#A-11029; Thermo Fischer Scientific); goat anti-rabbit IgG (H+L) Cy3 (Cat#111-165-003); donkey anti-goat IgG(H+L) Alexa Fluor 647 (Cat#705-605-147); donkey anti-chicken IgY(H+L) Cy3 (Cat#703-165-155); donkey anti-goat IgG (H+L) Cy3 (Cat#705-165-147); donkey anti-rabbit IgG (H+L) Cy3 (Cat#711-165-152); donkey anti-mouse IgG (H+L) Cy3 (Cat#715-165-150); donkey anti-rabbit IgG (H+L) Alexa Fluor 488 (Cat#711-545-152); donkey anti-mouse IgG(H+L) Alexa Fluor 488 (Cat#715-545-150). All from Jackson ImmunoResearch unless described otherwise. Antibodies were diluted in blocking buffer, used at a concentration of 1:400 and incubated for 1 hour at room temperature. For Sox10 staining additional amplification steps were performed using the following antibodies: donkey anti-goat IgG (H+L) biotin-streptavidin (Cat#705-065-003, Jackson ImmunoResearch) and peroxidase streptavidin (Cat#016-030-084, Jackson ImmunoResearch) and the TSA plus cyanine system (Cat#NEL744001 KT, Perkin-Elmer) according to manufacturer's guidelines. Nuclei were stained with Hoeschst 33342 (Cat#14533, Sigma-Aldrich) and slides were mounted in Fluorescent Mounting Medium (Cat#S3023, Dako). Imaging was performed using a DMI 6000B microscope (Leica).

Detection of Proliferation and Apoptosis Rates

To determine proliferation rates *in vivo*, animals were injected intraperitoneal with 2 μmol EdU (Cat#C10424, Thermo Fischer Scientific,) 1 hour prior to sacrifice. Histological sections were prepared as described above. For *in vitro* assays melanoma cells were pulsed with 10 μM EdU for one hour at 37°C. EdU detection was performed following manufacturer's instructions. To evaluate cell death the Annexin V Apoptosis detection Kit (Cat#556547, BD Pharmigen) was used according to manufacturer's guidelines. Proliferation and apoptosis *in vitro* were assed 48 hours post siRNA-mediated YY1 knockdown. Histological sections were evaluated by microscopy. Quantification of EdU incorporating or Annexin V positive cells in human cancer cell lines was performed by flow cytometry using a BD FACSCANTO II (BD Biosciences). FlowJo v7.6. was used for data analysis.

Protein Isolation and Western Blotting

Total protein isolation was performed in RIPA buffer (Cat#89900, Thermo Fischer Scientific) containing protease and phosphatase inhibitors (Cat#87786, Cat#78420, Thermo Fischer Scientific). SDS-PAGE was carried out in 4%–20% Mini-Protean TGX gels (Cat#456-1094, Bio RAD) and a total of 20 μg of protein was used. Nitrocellulose membranes were blocked in Odyssey blocking buffer (Cat#927-40000, Li-COR Biosciences) for 1 hour at room temperature. Primary antibodies, rabbit anti-YY1(D5D9Z) (Cat#46395, Cell Signaling Technology; 1:500), mouse anti-MITF (Cat#ab12039; Abcam, 1:500) and mouse anti-α Tubulin (Cat#T6070; Sigma-Aldrich; 1:2000) were diluted in Odyssey blocking buffer and incubated overnight at 4°C. Secondary antibodies donkey anti-mouse IgG IRdye 800 CW (Cat# 926-32212, Li-COR Biosciences), donkey anti-rabbit IgG, IRdye 680LT (Cat#926-68023, Li-COR Biosciences) and donkey anti-mouse IgG IRdye 680LT (Cat#926-68022, Li-COR Biosciences) were diluted in Odyssey blocking and incubated for 1 hour at room temperature. Blots were scanned and quantified with an Odyssey imaging system (Li-COR Biosciences).

RNA Isolation, Microarray, RNA-seq and qRT-PCR

Total RNA was isolated with RNAeasy mini kit (Cat#74106, QIAGEN) following manufacturer's instructions. This method was employed to isolate RNA for: qRT-PCR, RNA-seq and microarray analysis. For microarray and RNA-seq analysis, RNA was submitted to the Functional Genomics Center Zurich, University of Zurich. Microarray analysis of NCSCs and primed counterparts was performed in an Affymetrix GeneChip Mouse Genome 430 2.0 (GPL-1261) platform. RNAseq of E10.5 Control and Yy1 cko BAs was performed using the Illumina HiSeq 2000 platform. The same platform was used for RNA-seq analysis of human melanoma cells subjected to YY1 knockdown. RNA-seq of wild-type and *Tyr::Nras*^{Q61K};*Cdkn2a*$^{-/-}$competent melanocytes was performed at the iGE3 Genomics Platform, Geneva Switzerland using the Illumina HiSeq 4000 platform. Gene ontology networks were designed using ClueGo v2.3.2 (http://apps.cytoscape.org/apps/cluego) and Cytoscape v3.4.0 (https://cytoscape.org). Clusters with less than three nodes were omitted. For qRT-PCR, cDNA was synthesized by using Maxima First Strand cDNA Synthesis kit (Cat#K1641, Thermo Fischer Scientific) according to manufacturer's guidelines. qRT-PCR amplification was performed using SYBR Green I Master Mix (Cat#4707516001, Roche) with specific PCR primers for genes of interest, and RPL28 and β-actin as endogenous controls (Table S6). ChIP-qRT-PCR experiments were performed using primers described in Table S7. Measurements were performed on a LightCycler 480 System (Roche). qRT-PCR results are presented as the fold change over control and were calculated using the comparative delta delta Ct method.

ChIP-seq

Chromatin Immunoprecipitation (ChIP) was performed using Magna ChIP A/G kit (Cat#17-10085/86, Millipore) following manufacturer's instructions. Briefly, formaldehyde-fixed melanoma cells were lysed and subjected to sonication in order to generate DNA fragments raging from 300-700 bp. Sheared and cleared chromatin was incubated overnight with 5 μg of rabbit anti-Yy1 (H-414) antibody (Cat#sc-1703, Santa Cruz Biotechnology) or 5 μg rabbit anti-IgG antibody (Cat#sc-2027, Santa Cruz Biotechnology. Antibody-protein complexes were immunoprecipitated with A/G magnetic beads (Cat#17-10085/86, Magna ChIP, Millipore), washed, eluted, reverse crosslinked and treated with proteinase K (Cat#17-10085/86, Magna ChIP, Millipore). Libraries were performed by following Illumina TruSeq protocols and sequencing was performed at the iGE3 Genomics Platform, Geneva Switzerland.

All sequence reads were mapped using Bowtie 2 (http://bowtie-bio.sourceforge.net/bowtie2/index.shtml) into the hg19 UCSC reference human genome. Input samples were used as enrichment normalization control. Peak calling was performed with HOMER tool package (http://homer.ucsd.edu/homer/) using the "style=factor" option routinely used for TFs. Peak calling parameters were the following: L = 2 (filtering based on local signal), F = 2 (fold-change in target experiment over input control). AnnotatePeaks.pl was used to annotate peak position, and "makeUCSC file" was used to produce bedGraph formated files that were uploaded as custom tracks and visualized in the UCSC genome browser (http://genome.uscs.edu/). The experiment was performed twice in two independent biological replicates.

Oxygen Consumption Rate (OCR)

E10.5 Control and *Yy1* cko BA1 cells were isolated as described above and the number of live cells was determined by Trypan blue (Cat#T8154, Sigma-Aldrich) exclusion test. A total of 10000 live cells per well were seeded in fibronectin- coated XF^p cell plates (Cat#103022-100, Agilent), allowed to attach for 4 hours in BA1 maintenance media. Cells were rinsed once with media in order to discard non attached cells and incubated for one hour in non-buffered XF Base DMEM minimal medium (Cat#103334, Agilent) supplemented with 0.5mM sodium pyruvate (Cat#11360, Thermo Fischer Scientific), 5.5mM glucose (Cat#G7021, Sigma-Aldrich) and 2mM glutamine (Cat#25030, Thermo Fischer Scientific), pH7.4, in a 37°C incubator without $C0_2$. OCR was measured on a Seahorse XF^p Extra Flux Analyzer following manufacturer's instructions. Mitochondrial inhibitors were used at the following concentrations: 1 μM Oligomycin; 1 μM FCCP and 0.5 μM Antimycin A/Rotenone (103015-100, Agilent). OCR measurement in human melanoma cell lines subjected to YY1 KD was done in the same manner with the following exceptions: cells were transfected with Si-Ctrl and Si-YY1, after 24 hours cells were dissociated and plated in XFp plates and let to attach for 24 hours; and the concentration of glutamine used in the XF Base DMEM minimal medium was 4mM glutamine. Calculations of basal OCR, maximal respiratory capacity, ATP turnover were performed as previously (Varum et al., 2011).

Untargeted Metabolomics

Human melanoma cell lines were transfected with siRNA 48 hours previously to metabolite extraction. Cellular confluency was approximately 70%. Cells were rinsed with 75mM ammonium carbonate (207861, Sigma-Aldrich), pH7.4 and immediately frozen in liquid nitrogen. Metabolites were extracted by incubating cells with a 40:40:20 mix of acetonitrile (Cat#271004, Sigma-Aldrich): methanol (Cat#106009, Millipore): H20 for 10 minutes at −20°C. This procedure was repeated twice. Extracts were centrifuged at 4°C and resulting supernatants were frozen at −80°C until analysis. Quantification of metabolites was performed on an Agilent 6550 QTOF instrument by flow injection analysis time-of-flight mass spectrometry (Fuhrer et al., 2011). Detectable ions were putatively annotated by matching measured mass-to-charge ratios with theoretical masses of compounds listed in the human metabolome database v3.0 (http://www.hmdb.ca/) using a tolerance of 0.001 amu. Differentially abundant metabolites were categorized with the Small Molecule Pathway Database (http://smpdb.ca/).

Exogenous Metabolite Supplementation

Exogenous metabolites were added to melanoma growth media 24 hours post transfection and cells were maintained under these conditions for 24 hours. The following metabolites were used: Uridine (Cat#U3003, Sigma-Aldrich); Glutamic acid dimethyl ester (Cat#49560, Sigma-Aldrich); L-aspartic acid dimethyl ester (Cat#456233, Sigma-Aldrich); L-Carnitine hydrochloride (Cat#C0158, Sigma-Aldrich), Sodium pyruvate (Cat#11360, Thermo Fischer Scientific) and Nucleoside mix (Cat#ES-008-D, Millipore).

Protein Synthesis Rates

E11.5 Control and *Yy1* cko BA1 cells were isolated as described above and the number of live cells was determined by Trypan blue (Cat#T8154, Sigma-Aldrich) exclusion test. Equal number of live cells were plated in 96 wells fibronectin-coated plates, and let to attach for four hours as mentioned above. Media was discarded and cells were rinsed once with media in order to remove non-attached cells. Cells were pulsed with 20 μM of OP-Puro (Cat#Nu-931-5, Jena Bioscience) for 30 minutes at 37°C. OP-Puro detection was performed by using Click-IT Protein Synthesis Assay Kit (Cat#C10458, Thermo Fischer Scientific) following manufacturer's guidelines. To visualize DNA content cells were co-stained with PI/RNase solution (Cat#F10797, Invitrogen). The same protocol was applied to melanoma cells. In this case cells were pulsed with OP-Puro 48 hours post siRNA-mediated YY1 knockdown. A FACSCANTO II was used to perform flow cytometric analysis of OP-Puro fluorescence intensity. Of note, forward and side scatter gating was used to enrich for the live cell population and exclude debris.

Molecular Cloning

c-MYC was amplified from the pCDH-puro-cMYC plasmid (Cat#46970, Addgene) by using High Fidelity PCR master (Cat#2140314001, Roche) and using the following primers: Forward: 5'-ATT GGA ATT CTT ACG CAC AAG AGT TCC GTA G −3'- EcoRI and Reverse: 5'-ATG TAA GCT TAT GCC CCT CAA CGT TAG CTT −3'-Hind3. PCR product was purified from agarose gel using the QIAquick Gel extraction Kit (Cat#28704, QIAGEN). Restriction enzymes used to digest the PCR product and pMuLE-ENTR-CMV-L1-R5 vector (Cat#62090, Addgene) were EcoRI (Cat#ER0271, ThermoFisher Scientific) and Hind3 (Cat#ER0501, ThermoFisher Scientific) and ligation was performed with Anza T4 DNA ligase Master Mix (IVGN2108, ThermoFisher Scientific. L/R recombination of pMuLE-ENTR-CMV-cMYC-L1-R5, pMuLE-ENTR-SV40-eGFP-L5-L2 (Cat#62144, Addgene) and pLenti-X1-Piro-DEST (Cat#11297,

Addgene) was performed using Gateway LR Clonase II mix (CAT#11791020), as previously described (Albers et al., 2015). Ad-H1-Si-MITF and Ad-H1-Si-Control plasmids were previously described (Hoek et al., 2008).

Cell Transfections, Viral Production and Viral Transduction of Melanoma Cells

siRNA-mediated YY1 knockdown in human melanoma cell lines was achieved by employing jet prime transfection reagent (Cat#114-75, Polyplus) according to manufacturer's instructions. The siRNA used was: YY1HSS111432 (Invitrogen) with the following sequences CAUCUUAACACAUGCUAAGGCCAAA. A scrambled Si-RNA (Cat#12935, Thermo Fischer Scientific) was used as control. All experiments unless specified otherwise were carried out 48 hours after transfection. Standard calcium phosphate precipitation method was used to transfect HEK293T cells for lentiviral production. Packaging vectors used were psPAX2 (Cat#12260, Addgene) and pMD2.G (Cat#12259, Addgene). Supernatants containing viral particles were collected 48 hours and 72 hours post-transfection. Lentiviral transduction of melanoma cells was performed in medium containing viral particles and 8 μg/ml polybrene (Cat#H9268, Sigma-Aldrich). Adenoviral particles containing Ad-H1-Si-MITF and Ad-H1-Si-Control were a gift from Mitchel Levesque's laboratory. Melanoma cells were transduced with adenoviral vectors at a multiplicity of infection 200.

Integration of YY1, SOX10 and MITF Binding Sites

Peak calling for YY1, Sox10 and MITF ChIP-seq datasets was performed with MACS software (http://liulab.dfci.harvard.edu/MACS/) using p value cutoff of 0.05. Peak calls between YY1, SOX10, and MITF was intersected using bedTools to obtain A, B, C and D subsets. Peaks from YY1 ChIP-seq were extended to 5000 bp in each direction, and ChiP-seq signal for YY1 (in two replicates), SOX10 and MITF was visualized using SeqMINER (http://bips.u-strasbg.fr/seqminer/).

QUANTIFICATION AND STATISTICAL ANALYSIS

Information regarding n and statistical analysis used is described in each figure legend. Briefly, quantification of embryonic material was done in at least three control and *Yy1* cko embryos originating from two or more litters. To determine number of Dct+ cells per hair bulb during adult melanocyte homeostasis at least 100 hair bulbs from 3 or more animals were quantified per genotype. Quantification of skin melanomas was done at the time of sacrifice followed by GFP staining's to determine recombination status of the tumor. Annexin V and EdU quantifications in allografts were performed in five tumors. Cell culture-based experiments were done at least in three biological replicates. P values for comparison of two groups were calculated with unpaired Student's t test, whereas one-way ANOVA was used for multiple experimental groups. Kaplan-Meier curves p values were determined with Long-rank (Mantel-Cox) test. For metabolomics p values were calculated by two tailed, heteroscedastic t test and were adjusted for FDR according to the Benjamini-Hochberg procedure. $p < 0.05$ was consider significant. Graphpad Prism (https://www.graphpad.com) and MATLAB (https://ch.mathworks.com) software was used for statistical analysis.

DATA AND SOFTWARE AVAILABILITY

Datasets reported in this study deposited at ENA can be found at https://www.ebi.ac.uk/ena and have the following accession numbers: PRJEB21547 (RNA-seq comparing Control and Yy1 cko BA1 cell); PRJEB21636 (RNA-seq comparing Si-Control and Si-YY1 human melanoma cells); PRJEB21646 (ChiP-seq for YY1 in human melanoma cells); PRJEB30285 (RNA-seq comparing wild-type melanocytes versus $Nras^{Q61K}$;$Cdkn2a^{-/-}$ melanoma competent cells). Dataset deposited at GEO (Microarray comparing NCSCs and their primed counterparts) can be found at https://www.ncbi.nlm.nih.gov/geo/ and has the accession number GEO: GSE125480.